Supporting Information

Realizing One-Step Two-Electron Transfer of Naphthalene Diimides *via* a Regional Charge Buffering Strategy for Aqueous Organic Redox Flow Batteries

Zengrong Wang, Xu Liu, Xuri Zhang, Heng Zhang, Yujie Zhao, Yawen Li, Haiyan Yu and Gang He*

Abstract: Naphthalene diimide derivatives show great potential for application in neutral aqueous organic redox flow batteries (AORFBs) due to their highly conjugated molecular structure and stable two-electron storage capacity. However, the two-electron redox process of naphthalene diimides typically occurs via two separate steps with the transfer of one electron per step ("two-step two-electron" transfer process), which leads to an inevitable loss of voltage and energy. Herein, we report a novel regional charge buffering strategy that utilizes the core substituted electron-donating group to adjust the redox properties of naphthalene diimides, realizing two electrons transfer to occur via a single-step redox process ("one-step two-electron" transfer process). The symmetrical battery testing of **NDI-DEtOH** revealed exceptional intrinsic stability for lasting 11 days with a daily decay rate of only 0.11%. Meanwhile, AORFBs with **NDI-DMe/FcNCl** and **NDI-DEtOH/FcNCl** exhibited a remarkable 40% improvement in peak power density at 50% state of charge (SOC) in comparison to **NDI/FcNCl**-based AORFBs. In addition, the battery's energy efficiency increased by 24%, resulting in much more stable output power and significantly improved energy efficiency. These results are of great significance to practical applications of AORFBs.

Table of Contents

Experimental procedures

1. Materials and instrumentation

General. All reactions were performed using standard Schlenk and glovebox (Vigor) techniques under argon atmosphere. All chemicals were purchased from Energy Chemical Inc, and stored in an Argon glovebox. Column chromatographic purification of products was accomplished using 200-300 mesh silica gel.

NMR spectra were recorded on a spectrometer operating at 400 MHz for ^{1}H and 100 MHz for ^{13}C NMR spectra on a Bruker ascend spectrometer (Bruker, Zurich, Switzerland). Coupling constants were reported in Hz with multiplicities denoted as s (singlet), d (doublet), t (triplet), q (quartet) and m (multiplet). UV-vis measurements were performed using a Lambd 950 absorption spectrophotometer (OceanOptics, Florida, USA). The cyclic voltammetry (CV) and differential pulse voltammetry (DPV) in solution were measured using CHI660E-B157216. The Linear sweep voltammetry (LSV) was measured on a rotating disk electrode (RDE) device (Pine Instruments Co., North Carolina, USA, 0.1963 cm^2). All battery tests were conducted under an Ar atmosphere. The flow battery was tested at room temperature on the Neware battery test system (CT-4008T-5V12A-S1-F, Shenzhen, China). All photographs were taken using a Nikon D5100 digital camera. Flow battery test fixture and graphite felt were purchased from Wuhan Zhisheng New Energy Co., Ltd (Wuhan, China). The DSV anion-exchange membrane was purchased from Shanghai TsingRoss Environmental Technology Co., Ltd (Shanghai, China), with film thickness (95 μm), burst strength (150 kPa), pore diameter (1∼3 nm), and area-specific resistance (1.1 Ω cm^2 for 0.5 M NaCl). The peristaltic pump (BT100M) was purchased from Baoding Chuang Rui Precision Pump Co., Ltd (Baoding, China).

The Polarizable Continuum Model (PCM) as a self-consistent reaction field (SCRF) was used for the calculation of equilibrium geometries, vibrational frequencies and excited state calculations. The geometries for the ground state of these compounds were optimized at the B3LYP hybrid functional and 6-311+G(d) basis set for all atoms. The calculated oscillator strength (f), molecular orbitals (MOs) involved in the main transitions were reported in this work. It should be pointed out that the structures of all stationary points were fully optimized, and frequency calculations were performed at the same level. The frequency calculations confirmed the nature of all revealed equilibrium geometries: there were no imaginary frequencies. All of the above computational calculations reported in this work were performed using the Gaussian 09 code.[1] The structure for optimized molecules was measured by Mercury. The ADCH charge and spin density plots were calculated by the Multiwfn code.[2]

The batteries were assembled with two steel plates, two polytetrafluoroethylene insulation plates, two Cu plate collectors, two graphite plates, and two graphite-felts, which was separated by DSV membrane. The battery has an active area of 4 cm^2. For full battery tests, 0.1 M anode material was dissolved in 2 M NaCl (6 mL) and 0.1 M cathode material was dissolved in 2 M NaCl (15 mL). When AORFBs were tested at a higher concentration (0.5 M), the concentration of NaCl was 1 M. In the symmetric batteries, 0.1 M electrolyte (NDI-DMe^{2+} or NDI-$DEtOH^{2+}$) concentration in 2.0 M NaCl aqueous solution with 6.0 mL as capacity-limiting side and 8.0 mL 0.1 M electrolyte (NDI-DMe^{0} or NDI-$DEtOH^{0}$) as noncapacity-limiting side, respectively.The electrolytes were pumped into the cell at a flow rate of 60 mL min^{-1} through a peristaltic pump (BT100M, Baoding Chuang Rui Precision Pump Co., Ltd.). The reservoirs were purged with Ar to displace any O_2 in the system, and then sealed. The flow cell was galvanostatically using a Neware battery test system in the glove box at RT. The flow battery was conducted at current densities from 20 to 100 mA cm^{-2}. The extended cycling experiment was operated at 40 mA cm^{-2}. For polarization testing, after the initial few stable cycles of the battery, charge at a low current density of 10 mA/cm^2 to 100% SOC state, with a cut-off voltage of 1.6 V, and then discharge at 10, 20, 30, 40... 400 mA/cm^2. After each discharge, fully charge at 10 mA/cm^2. The cut-off voltage of 50% SOC is about 1.1 V which depends on the specific voltage corresponding to the battery charging to 50% of the actual capacity. The average voltage and current data collection operation remains consistent.

In symmetric battery, 0.1 M NDI-derivates (6.0 mL) was fully charged with a current density of 10 mA cm^{-2} to a highly reduced state (100% SOC) against the excess 0.1 M FcNCl (15 mL), which was used as a catholyte. And then the FcNCl side was washed with deionized water and refilled with fresh 0.1 M NDI-derivates (8 mL) as anolyte.

2. Synthetic procedures and characterization data

2.1 The synthesis of core-substituted naphthalimide derivatives

2.1.1 Synthesis of 2,6-dibromo-1,4,5,8-naphthalenetetracarboxylic dianhydride (2Br-NDI):

Compounds **2Br-NDI** was prepared according to the previous report.[3] 10.72 g (39.97 mmol) naphthalene-1,4,5,8-tetracarboxylicdianhydride (NTDA) was slurried with 100 mL concentrated sulfuric acid (98%) in a 250 ml double-necked round bottom flask at room temperature. 17.14 g (59.96 mmol) 5,5-dimethyl-1,3-dibromohydantoin (DBH) was added to the slurry by four portions within an hour at room temperature. Then the was heated with magnetic stirring at 60 ºC for 12 h. The resulting mixture was poured into a beaker filled with crushed ice to precipitate the solid. The precipitated solid was washed with water and acetone, then dried overnight to obtained a yellow solid (12.0 g, 70%). The product will be used without further purification.

2.1.2 Synthesis of N,N'-bis((dimethylamino)propylamino)-2,6-dibromo-1,4,5,8-naphtalenediimide (N2):

Compound **N2** was synthesized according to the reported method.[4] 2Br-NDI (4 g, 9.39 mmol) was dispersed with 90 mL acetic acid in a 200 mL Schlenk-flask under nitrogen. Dimethylaminopropylamine (2.4 g, 23.44 mmol) was slowly added to the reaction mixture with stirring at room temperature. The mixture was heated at 130 ºC for 30 min. After the reaction, the resulting crimson solution was diluted with 200 mL water, neutralized with NaOH, and after the solution recovered to rt and extracted with CH_3Cl. The crude orange product was purified by chromatography on a silica gel column (CH_2Cl_2/MeOH,10:1, with 1% Et_3N) to yield **N2** (2.3 g, 40%) as golden yellow solid. **^{1}H NMR** (400 MHz, $CDCl_3$) δ 8.99 (s, 2H), 4.31-4.21 (m, 4H), 2.44 (t, J = 7.0 Hz, 4H), 2.23 (s, 12H), 1.95-1.85 (m, 4H). **^{13}C NMR** (100 MHz, $CDCl_3$) δ 160.80, 139.02, 128.30, 127.73, 125.36, 124.13, 57.18, 45.39, 39.99, 25.67.

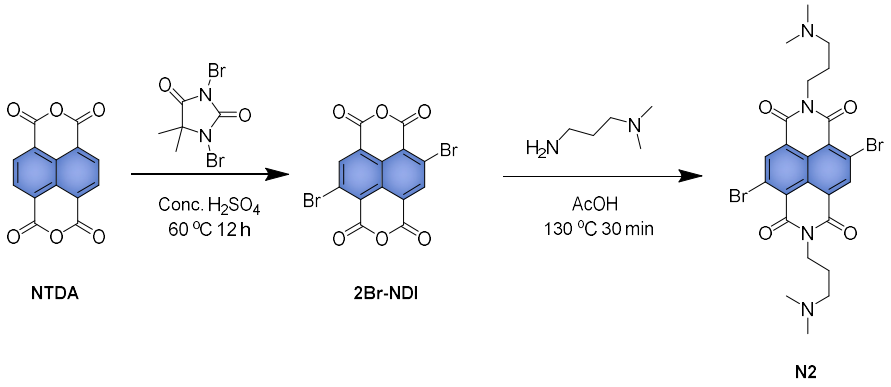

Scheme S1. The synthesis route of **N2.**

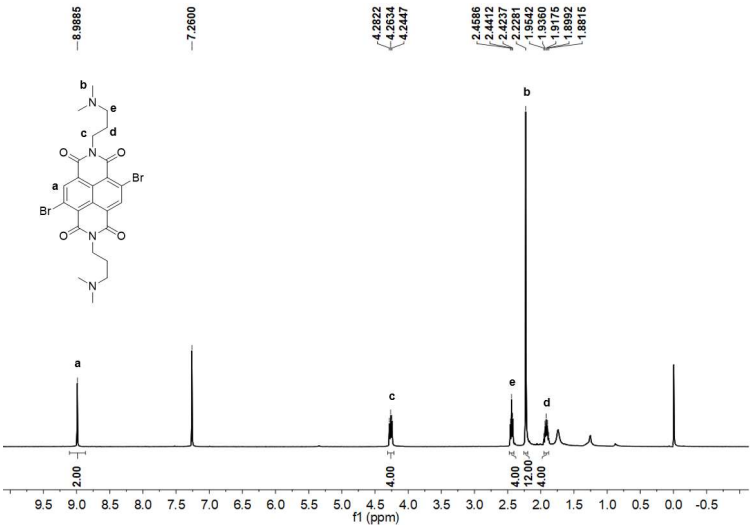

Figure S1. ^{1}H NMR ($CDCl_3$, 400 MHz) spectrum of **N2**

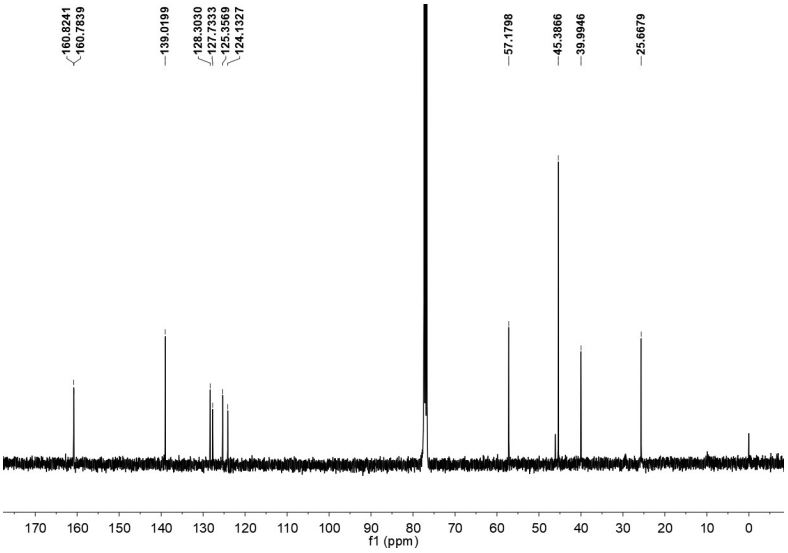

Figure S2. ^{13}C NMR ($CDCl_3$, 100 MHz) spectrum of **N2**

2.1.3 Synthesis of N,N'-bis((dimethylamino)propylamino)-2,6-bis(dimethylamino)-1,4,5,8-naphthalenetetracarboxylic dianhydride (N3):

In a 100 mL Schlenk flask, **N2** (4 g, 6.74 mmol) was added in 40 mL of dimethylamine in THF (2 M) under nitrogen, then the mixed solution was stirred and refluxed at 85 ºC for 24 h. The resulting solution was concentrated in a rotary evaporato to obtained crude product, then the crude product was dissolved in 50 mL trichloromethane and extracted with alkali water, collected the organic phase, and evaporated in vacuo to obtain **N3** (3.3 g, 94%) as blue solid. **^{1}H NMR** (400 MHz, $CDCl_3$) δ 8.99 (s, 2H), 4.30-4.25 (m, 4H), 2.44 (t, J = 7.0 Hz, 4H), 2.23 (s, 12H), 1.95-1.85 (m, 4H). **^{13}C NMR** (100 MHz, $CDCl_3$) δ 160.80, 139.02, 128.30, 127.73, 125.36, 124.13, 57.18, 45.39, 39.99, 25.67.

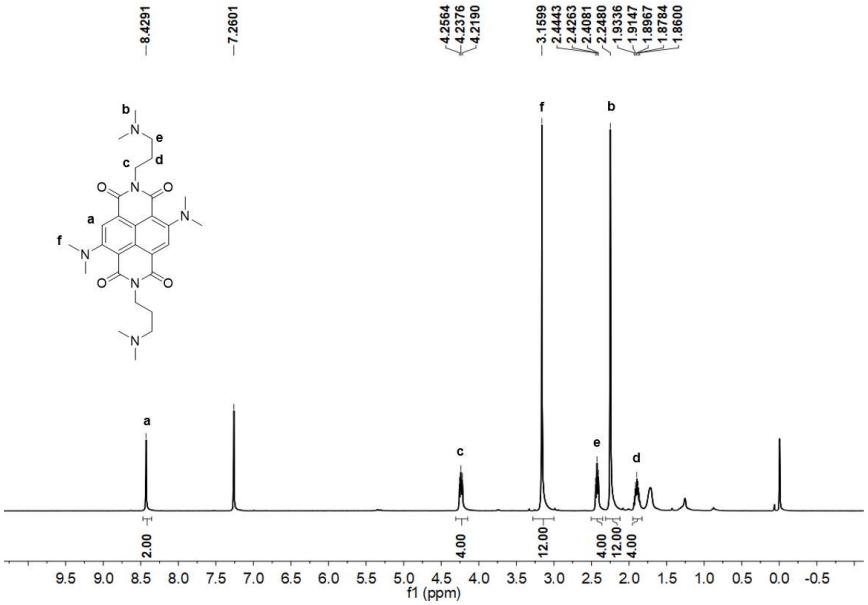

Figure S3. ^{1}H NMR ($CDCl_3$, 400 MHz) spectrum of **N3**

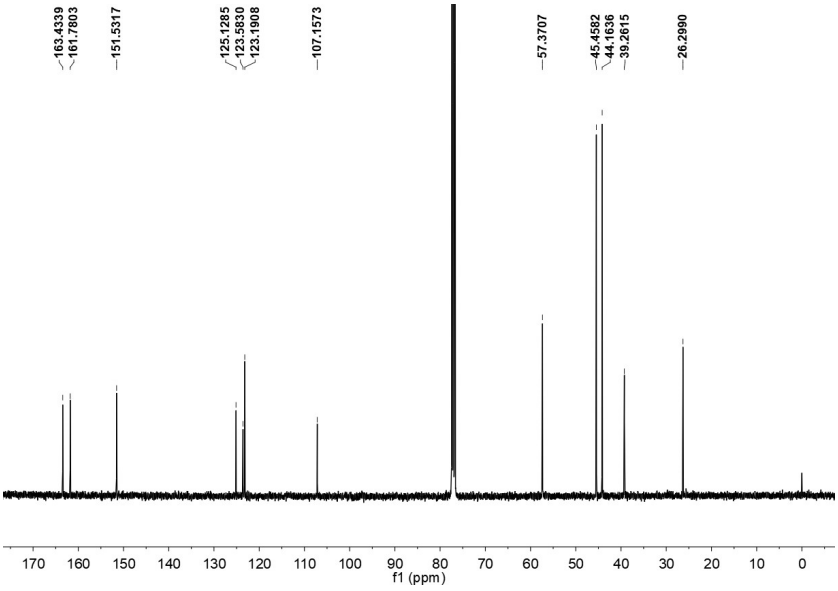

Figure S4. ^{13}C NMR ($CDCl_3$, 100 MHz) spectrum of **N3**

2.1.4 Synthesis of N,N'-bis((trimethylamino)propylamino)-2,6-bis(dimethylamino)-1,4,5,8-naphthalenetetracarboxylic dianhydride dichloride (NDI-DMe):

In a 100 mL Schlenk flask, the **N3** (4 g, 7.65 mmol) was dissolved in a 30 mL solution of chloromethane (1 M in THF) under nitrogen, the reaction mixture was heated at 85 ºC for 12 h. The product was collected by filtration, washed with dichloromethane and dried under vacuum. A blue solid (4.5 g, 95%). **^{1}H NMR** (400 MHz, D_2O) δ 7.92 (s, 2H), 4.08 (t, J = 6.8 Hz, 4H), 3.51-3.44 (m, 4H), 3.12 (s, 18H), 2.99 (s, 12H), 2.20-2.15 (m, 4H). **^{13}C NMR** (100 MHz, D_2O) δ 163.90, 161.24, 151.25, 123.29, 122.51, 122.21, 105.08, 64.10, 53.21, 43.29, 37.43, 21.59.

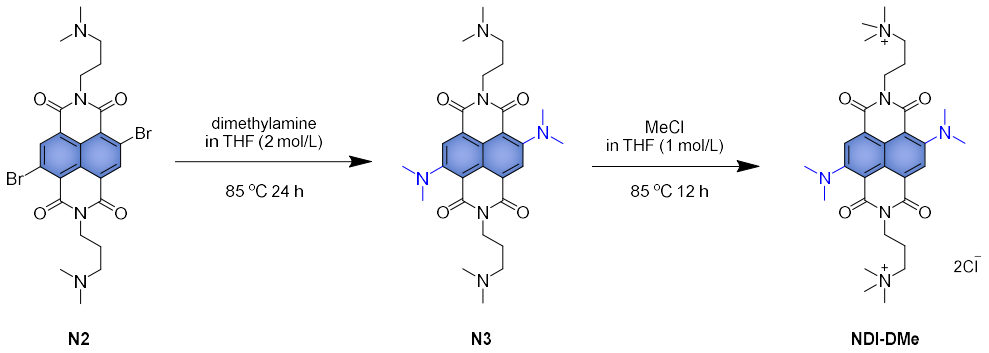

Scheme S2. The synthesis route of **NDI-DMe.**

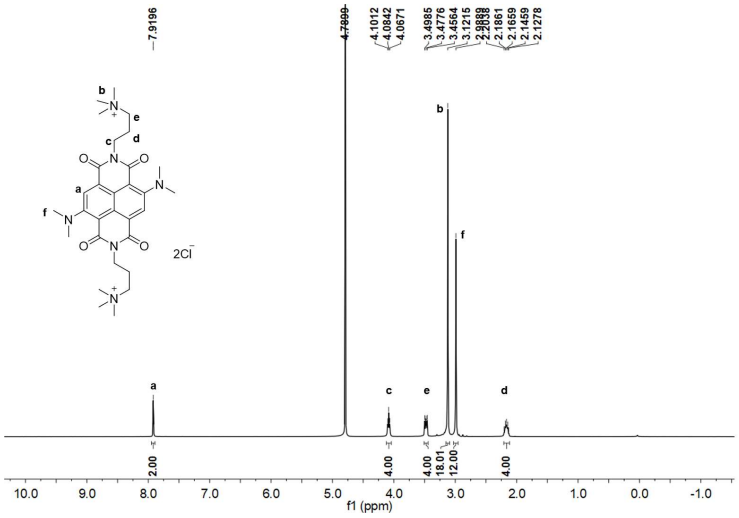

Figure S5. ^{1}H NMR (D_2O, 400 MHz) spectrum of **NDI-DMe**

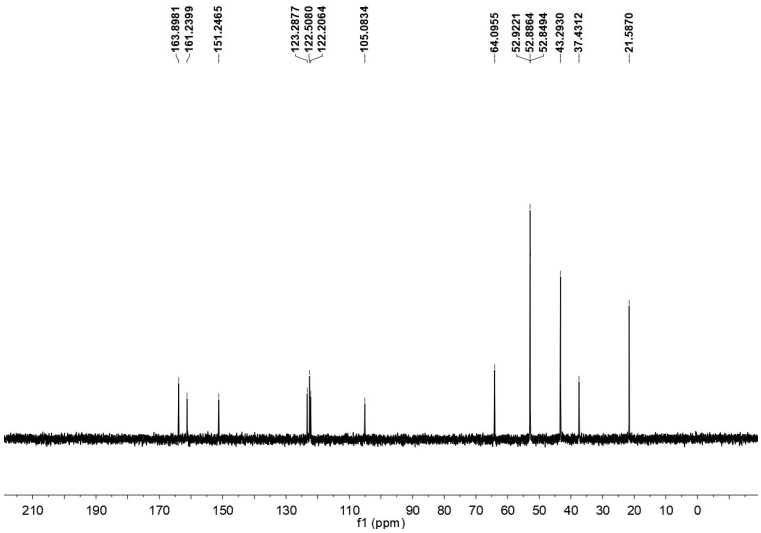

Figure S6. ^{13}C NMR (D_2O, 100 MHz) spectrum of **NDI-DMe**

2.1.5 Synthesis of N,N'-bis((trimethylamino)propylamino)-2,6-bis((2-hydroxyethyl)amino)-1,4,5,8-naphthalenetetracarboxylic dianhydride (N4):

In a 200 mL Schlenk flask, **N2** (2 g, 3.37 mmol) was dispersed in 60 mL 2-methoxyethanol, then dihydroxyethylamine (15.36 g, 146.1 mmol) was added in the mixture, heated at 130 °C for 18 h. The resulting blue solution was concentrated in a rotary evaporator and purified by crystallisation from acetone as a blue solid (2 g, 92%). **^{1}H NMR** (400 MHz, $CDCl_3$) δ 8.55 (s, 2H), 4.21 (t, J = 7.1 Hz, 4H), 3.70 (s, 16H), 2.39 (t, J = 7.1 Hz, 4H), 2.23 (s, 12H), 1.90-1.85 (m, 4H). **^{13}C NMR** (100 MHz, $CDCl_3$) δ 163.36, 162.96, 152.43, 129.13, 125.63, 124.48, 112.41, 59.38, 57.00, 55.34, 45.26, 39.19, 26.16.

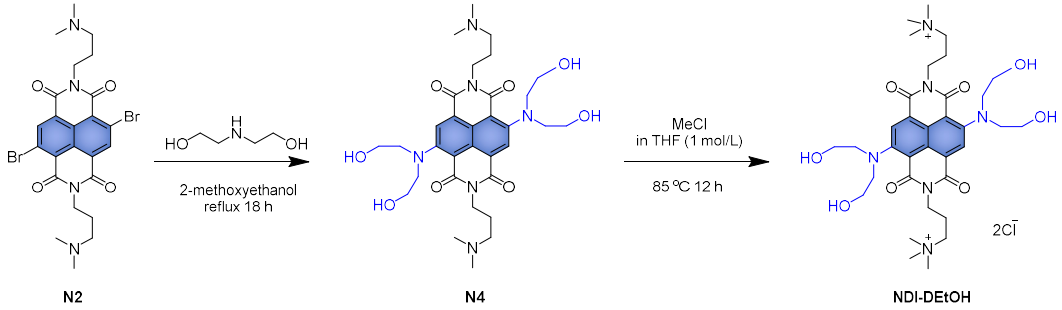

Scheme S3. The synthesis route of **NDI-DEtOH.**

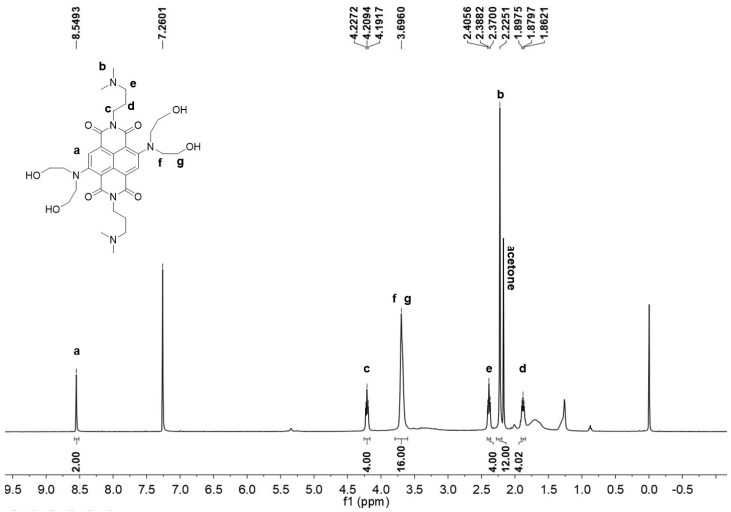

Figure S7. ^{1}H NMR ($CDCl_3$, 400 MHz) spectrum of **N4**

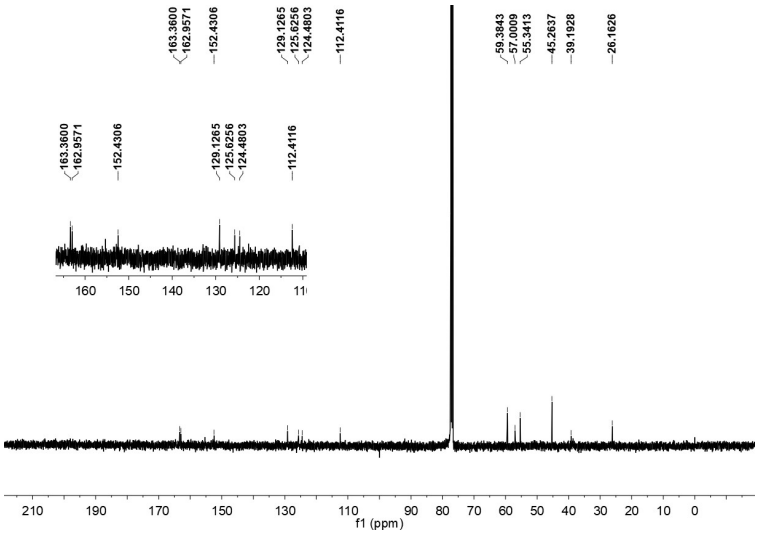

Figure S8. ^{13}C NMR ($CDCl_3$, 100 MHz) spectrum of **N4**

2.1.6 Synthesis of N,N'-Bis((trimethylamino)propylamino)-2,6-bis((2-hydroxyethyl)amino)-1,4,5,8-naphthalenetetracarboxylic dianhydride dichloride (NDI-DEtOH):

In a 100 mL Schlenk flask, the **N4** (3 g, 4.67 mmol) was dissolved in a 20 mL solution of chloromethane (1 M in THF) under nitrogen, the reaction mixture was heated at 85 ºC for 12 h. The product was collected by filtration, washed with dichloromethane and dried under vacuum. A blue solid (3.26 g, 94%). **^{1}H NMR** (400 MHz, D_2O) δ 8.52 (s, 2H), 4.21 (t, J = 6.8 Hz, 4H), 3.75 (t, J = 5.0 Hz, 8H), 3.64 (d, J = 23.3 Hz, 8H), 3.50-3.45 (m, 4H), 3.11 (s, 18H), 2.28-2.18 (m, 4H). **^{13}C NMR** (100 MHz, D_2O) δ 163.9, 162.23, 152.12, 126.81, 124.33, 123.49, 109.00, 64.11, 58.54, 53.93, 53.24, 48.83, 42.85, 37.62, 21.59.

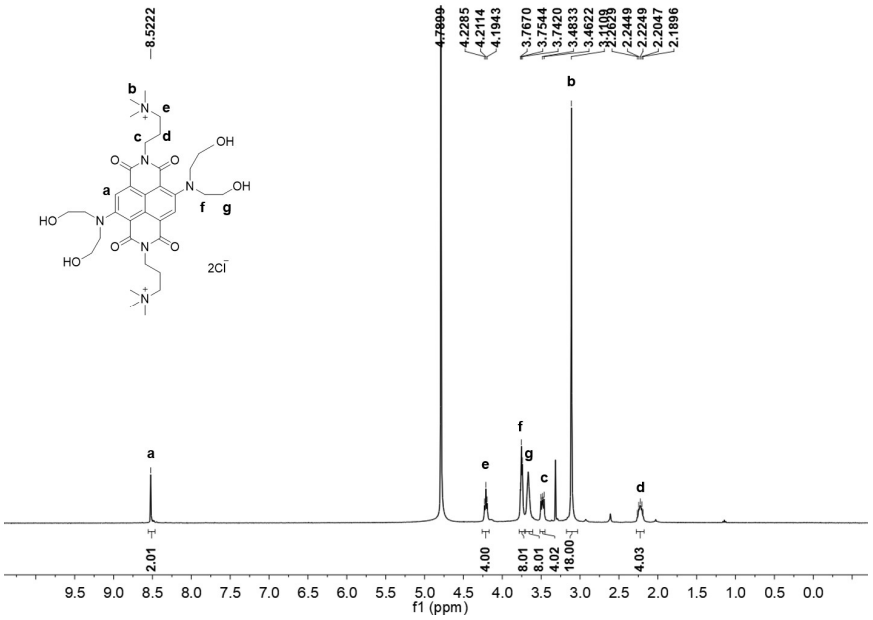

Figure S9. ^{1}H NMR ($CDCl_3$, 400 MHz) spectrum of **NDI-DEtOH**

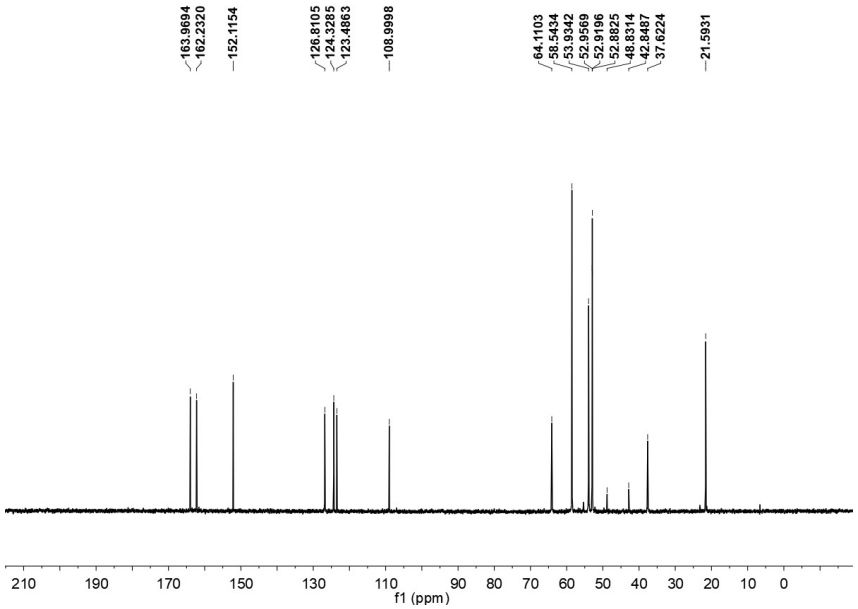

Figure S10. ^{13}C NMR ($CDCl_3$, 100 MHz) spectrum of **NDI-DEtOH**

2.1.6 Synthesis of N,N'-Bis((trimethylamino)propylamino)-1,4,5,8-naphthalenetetracarboxylic dianhydride dichloride (NDI)

This compound was synthesized according to the reported procedures.[5] ^{1}H NMR (400 MHz, D_2O): δ 8.60 (s, J = 2.4 Hz, 4H), 4.23 (t, J = 6.9 Hz, 4H), 3.55-3.50 (m, 4H), 3.14 (s, 18H), 2.30-2.25 (m, 4H). ^{13}C NMR (100 MHz, D_2O): δ 163.47, 131.00, 125.57, 125.46, 63.95, 52.96, 37.70, 21.38.

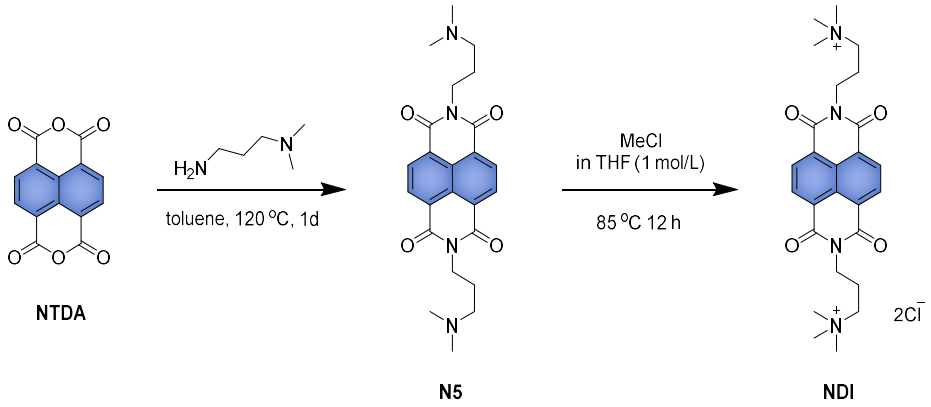

Scheme S4. The synthesis route of **NDI.**

2.2 HRMS spectra

2.2.1 HRMS of N3

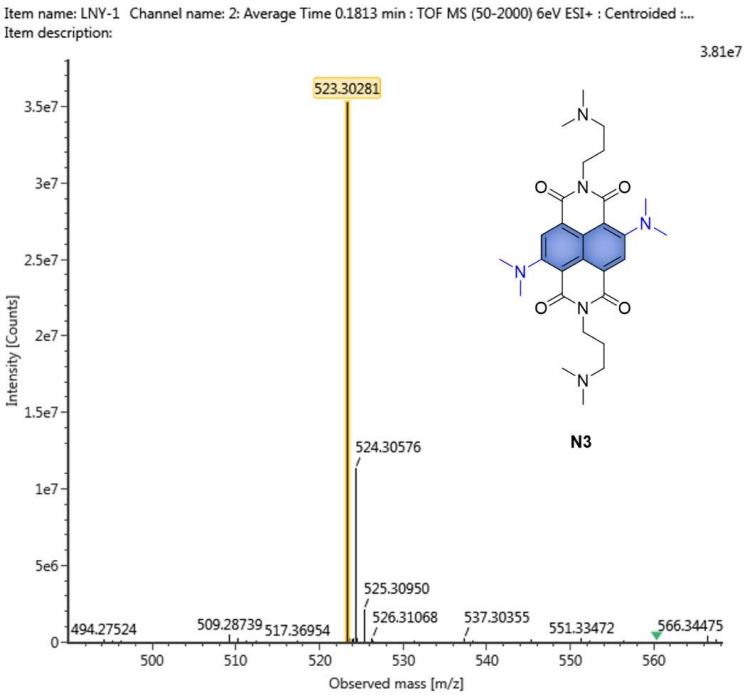

Figure S11. HRMS of **N3**

2.2.2 HRMS of NDI-DMe^{2+}

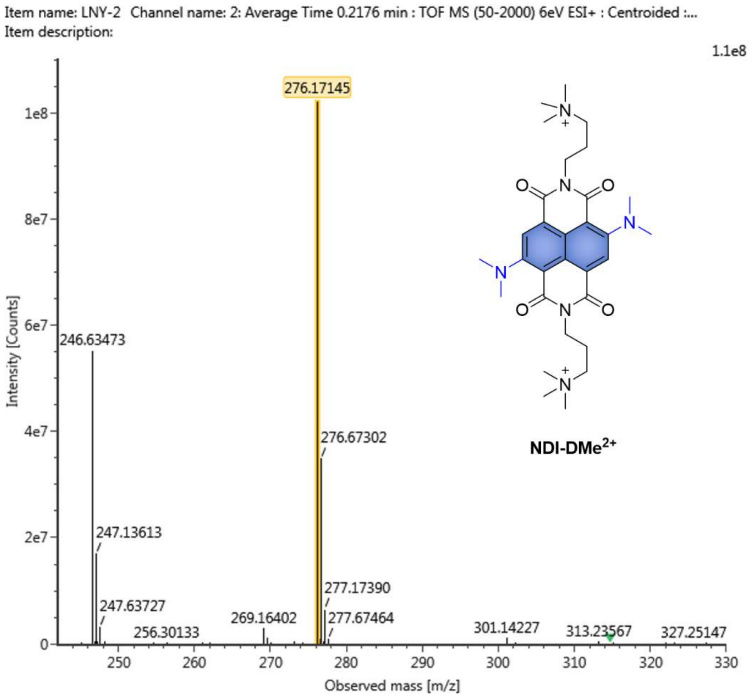

Figure S12. HRMS of NDI-DMe^{2+}

2.2.3 HRMS of N4

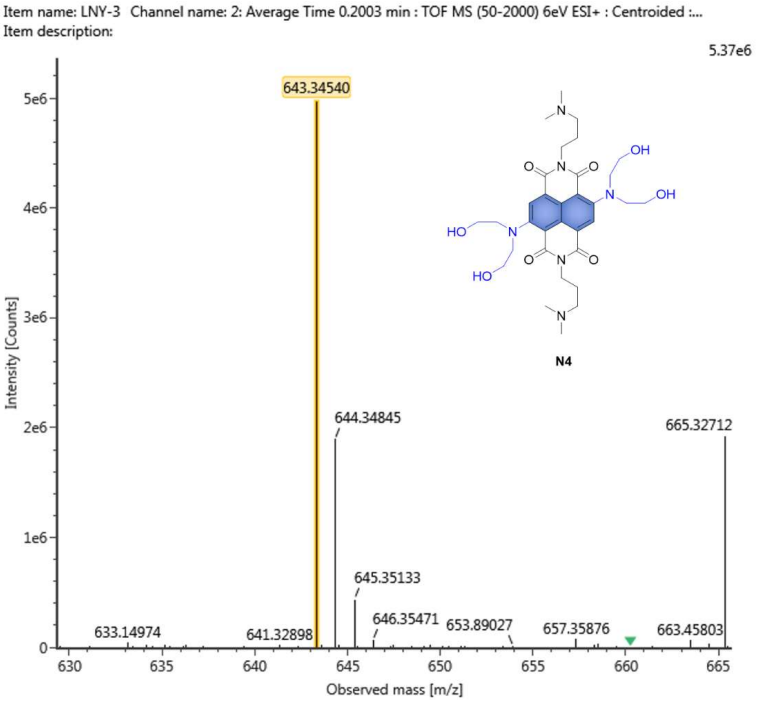

Figure S13. HRMS of **N4**

2.2.4 HRMS of NDI-DEtOH^{2+}

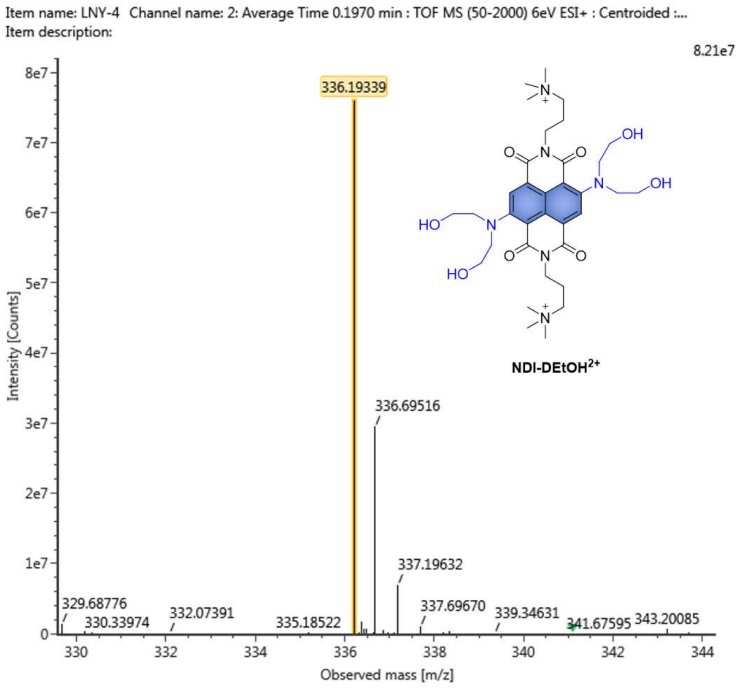

Figure S14. HRMS of **NDI-DEtOH^{2+}**

3. Solubility tests

The solubility of **NDI-DMe** and **NDI-DEtOH** was tested in water by UV-vis spectra.[6] Firstly, a standard solution of sample was prepared and measured the absorbance curve, then the standard solution was diluted step by step and absorbance curves of the solution at different concentrations were measured to obtained the absorbance-concentration standard curve. The saturated solution of the sample was prepared and its absorbance curve was obtained after dilution in a certain proportion. Finally, the solubility of the sample was calculated according to the standard absorbance curve.(**NDI-DMe**: 0.92 M in H_2O, 0.612 M in 2 M NaCl; **NDI-DEtOH**: 0.94 M in H_2O, 0.65 M in 2 M NaCl).

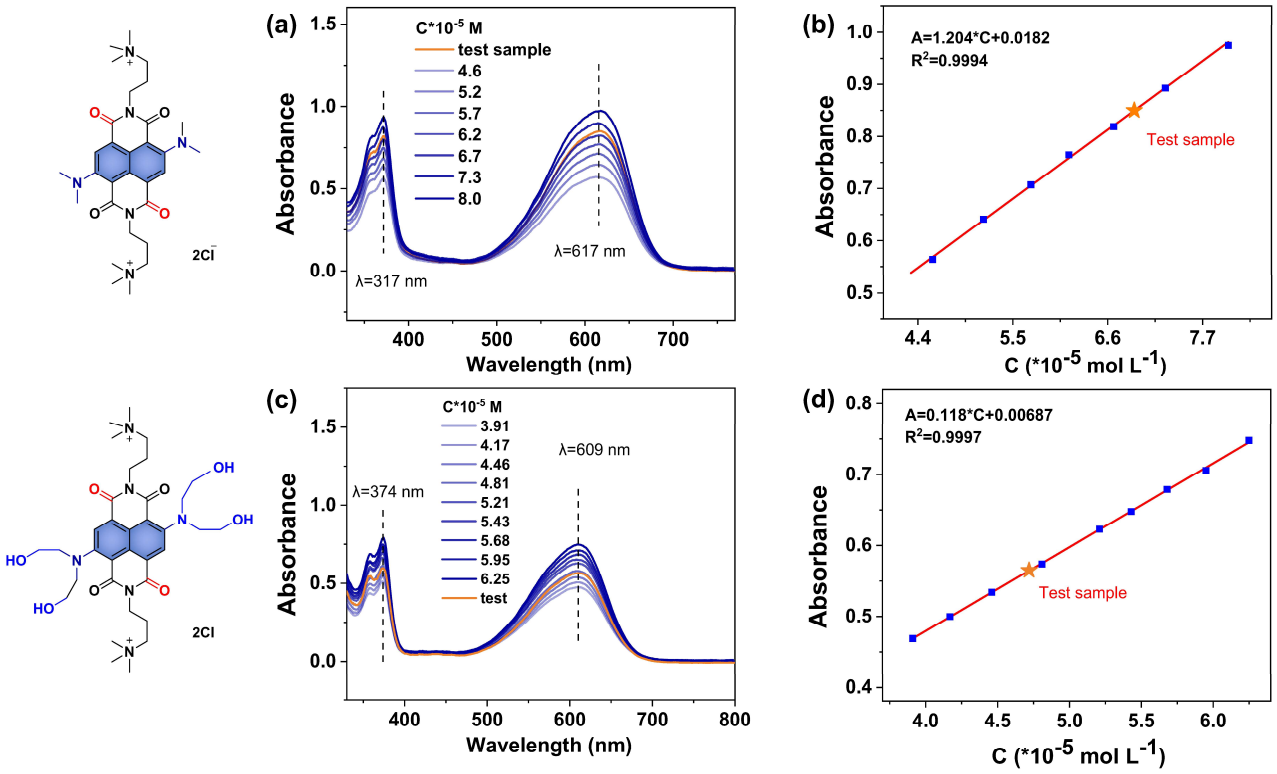

Figure S15. UV-vis calibration lines for determination of the solubility of **NDI-DMe**, **NDI-DEtOH**. UV-vis spectra for (a) **NDI-DMe**, (c) **NDI-DEtOH** at different concentrations in water. The absorbance *versus* the concentration for (b) **NDI-DMe** at 617 nm, (d) **NDI-DEtOH** at 609 nm.

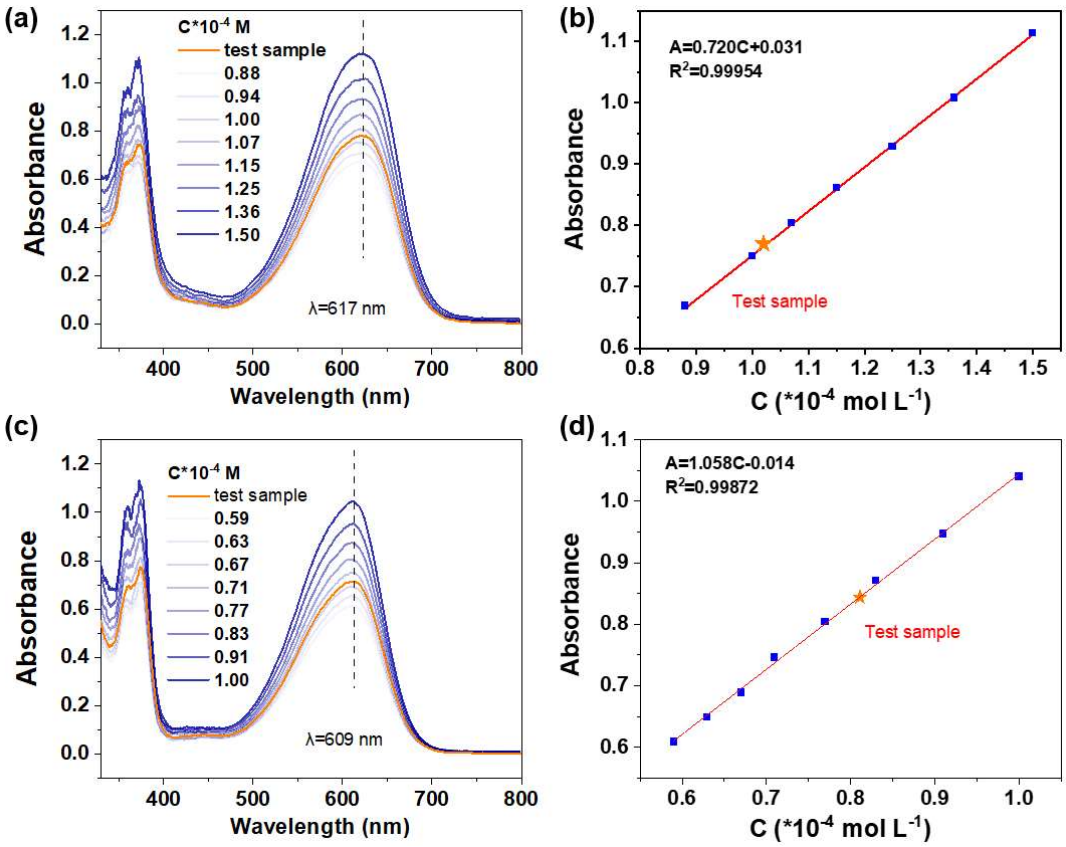

Figure S16. UV-vis calibration lines for determination of the solubility of **NDI-DMe**, **NDI-DEtOH**. UV-vis spectra for (a) **NDI-DMe**, (c) **NDI-DEtOH** at different concentrations in 2 M NaCl solution. The absorbance *versus* the concentration for (b) **NDI-DMe** at 617 nm, (d) **NDI-DEtOH** at 609 nm.

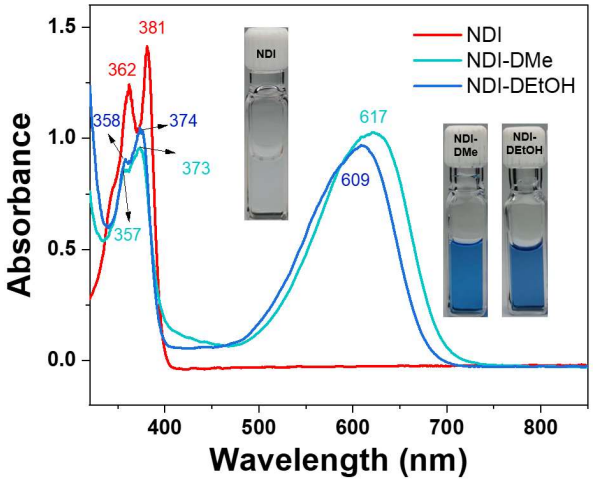

Figure S17. UV-vis spectra and optical photograph of **NDI**, **NDI-DMe,** and **NDI-DEtOH** in water.

4. The cyclic voltammogram (CV) and differential pulse voltammetry (DPV) tests

All the cyclic voltammetry and differential pulse voltammetry tests were carried out in 0.5 M NaCl electrolyte solutions. Redox potential was referenced to NHE. The glassy carbon electrode (d=3 mm) was used for the working electrode. The platinum sheet (1 cm^2) was used for the counter electrode. The reference electrode consisted of a silver wire coated with a layer of AgCl and suspended in a solution of 3 M KCl electrolyte (Ag/AgCl, *vs.* NHE).

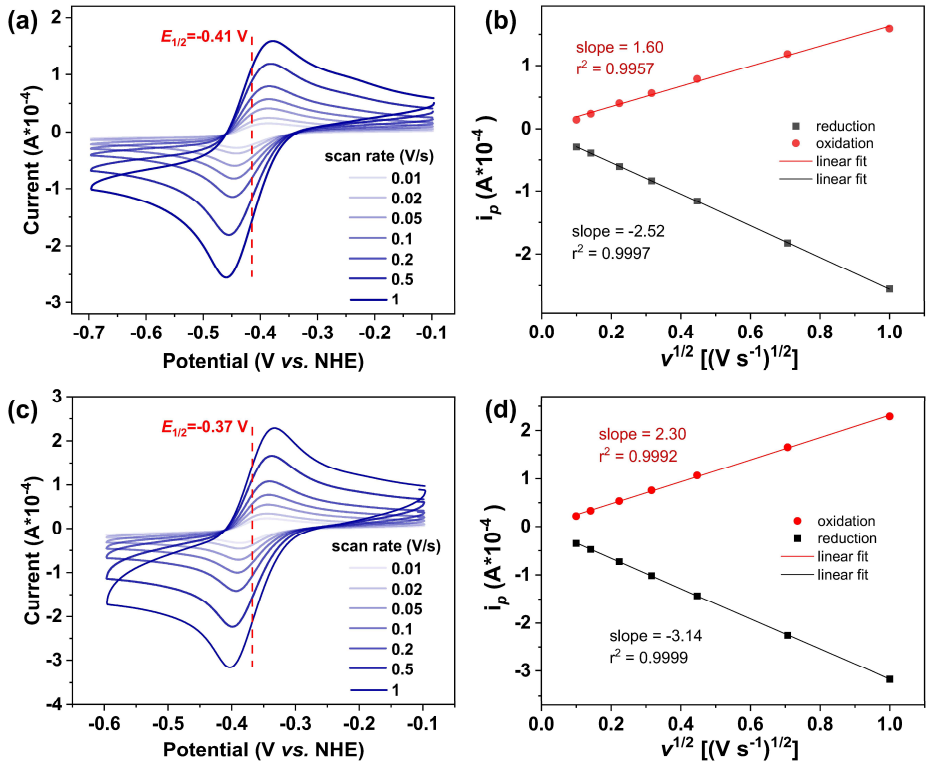

Figure S18. The cyclic voltammogram at different scan rates from 0.01 V s^{-1} to 1 V s^{-1}; conditions: 4.0 mM (a) **NDI-DMe**, (c) **NDI-DEtOH** in 0.5 M NaCl electrolyte. The plot of peak current (i_p) over the square root of scan rates ($v^{1/2}$) for (b) **NDI-DMe,** (d) **NDI-DEtOH**.

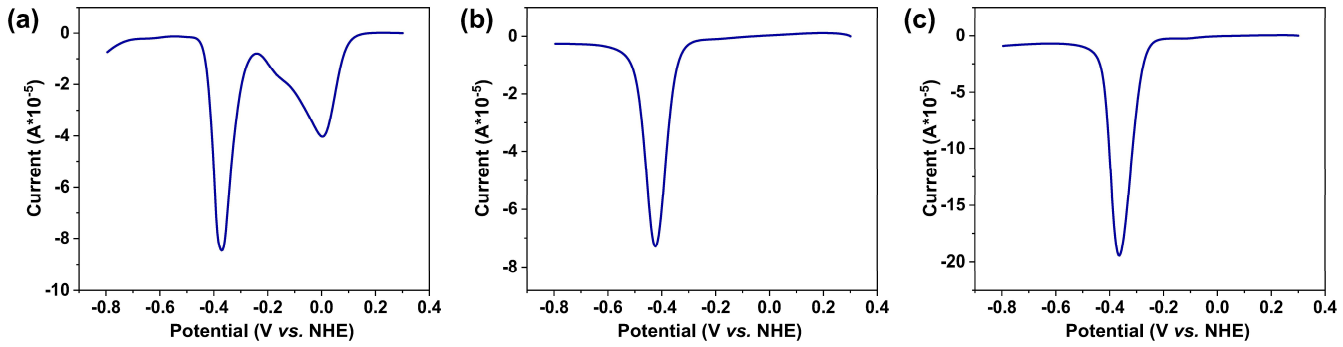

Figure S19. The differential pulse voltammetry with potential increment of 0.004 V; conditions: 4.0 mM (a) **NDI**, (b) **NDI-DMe**, (c) **NDI-DEtOH** in 0.5 M NaCl electrolyte.

5. The electrochemical kinetics studies

All linear sweep voltammetry (LSV) studies were conducted using a CHI660E electrochemical workstation and with a three-electrode configuration. A glassy carbon rotating electrode (5 mm diameter) was used as the working electrode along with a platinum sheet counter electrode and an Ag/AgCl reference electrode same as used in LSV studies. Before data collection, the electrolyte was purged by Ar for 20 minutes to remove the oxygen dissolved in the electrolyte. LSV scans were recorded at a scan rate of 5 mV s^{-1}.

The diffusion coefficient (D, cm^2 s^{-1}) was determined by the slope of the fitted Levich equation (eq 1).

$$i_l = 0.620nFAcD^{2/3}v^{-1/6}\omega^{1/2} \quad (1)$$

where i_l was the mass transfer limiting current from RDE tests, n was the electron transfer number, Faraday's constant F = 96485 C mol^{-1}, electrode area A = 0.1963 cm^2, concentration c = 1×10^{-6} mol cm^{-3}, kinetic viscosity v = 9×10^{-3} cm^2 s^{-1} (0.5 M NaCl aqueous solution), ω represented rotate speed (rad/s).

The electron transfer constant (k_0, cm s^{-1}) was calculated from the Koutecký-Levich equation (eq 2).

$$i^{-1} = {i_l}^{-1} + {i_k}^{-1} = (0.620nFAcD^{2/3}v^{-1/6}\omega^{1/2})^{-1} + (nFAk_0c)^{-1} \quad (2)$$

where i represented the measured current, i_k was the kinetic current (no mass transfer), which can be obtained from the butler-volmer equation (eq 3).

$$\eta = \frac{2.303RT}{\alpha nF}\log i_0 - \frac{2.303RT}{\alpha nF}\log i \quad (3)$$

where η represented over potential, i_0 was the exchange current, α was the transfer coefficient, R is the universal gas constant (8.314 J K^{-1} mol^{-1}), and T is the temperature (298 K). When η was equal to 0, i_0 can be obtained and k_0 can be calculated by the following equation (eq 4).

$$k_0 = \frac{i_0}{nFAc} \quad (4)$$

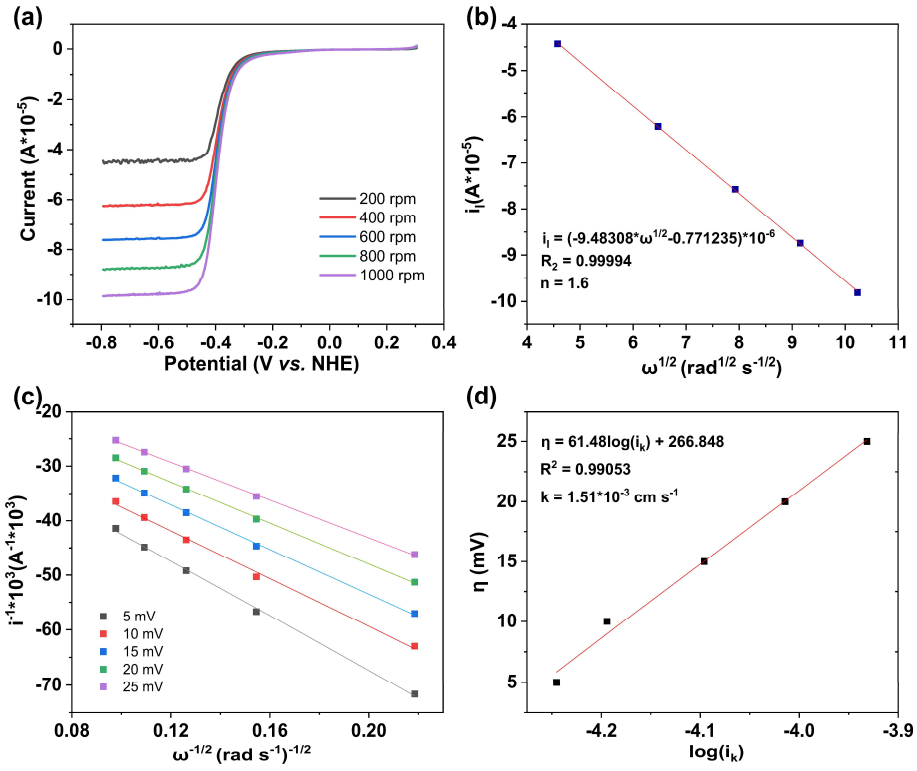

Figure S20. LSV measurements of 1 mM **NDI-DMe** in 0.5 M NaCl. (a). The limiting current *versus* potential at different rotation rates and potential sweeping rate of 5 mV s^{-1}. (b) Levich plot (i^{-1} *vs.* $\omega^{1/2}$) of **NDI-DMe**. (c) Koutecký-Levich plot (i^{-1} *vs.* $\omega^{-1/2}$) of **NDI-DMe** at different overpotentials. (d) Tafel plot (η *vs.* logi_k) of **NDI-DMe**.

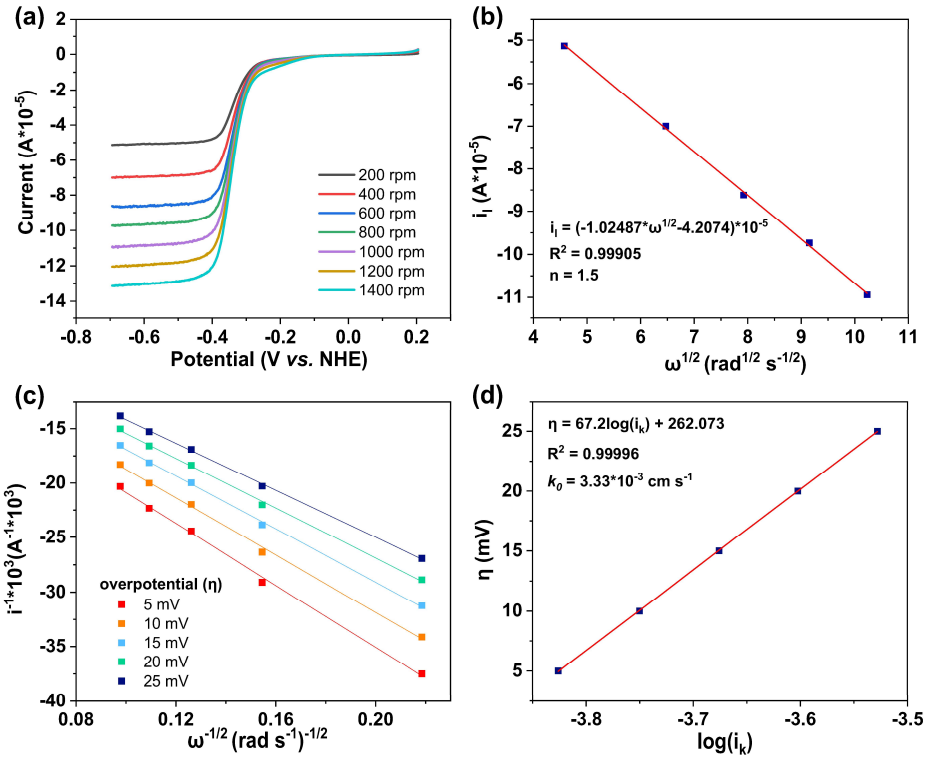

Figure S21. LSV measurements of 1 mM **NDI-DEtOH** in 0.5 M NaCl. (a). The limiting current *versus* potential at different rotation rates and potential sweeping rate of 5 mV s^{-1}. (b) Levich plot (i^{-1} *vs.* $\omega^{1/2}$) of **NDI-DEtOH**. (c) Koutecký-Levich plot (i^{-1} *vs.* $\omega^{-1/2}$) of **NDI-DEtOH** at different overpotentials. (d) Tafel plot (η *vs.* $\log i_k$) of **NDI-DEtOH**.

Table S1. Electrochemical data of **NDI**, **NDI-DMe** and **NDI-DEtOH**.

Compound	$E_{1/2}$(V *vs.* NHE)	Diffusion coefficient (D, cm^2 s^{-1})	Apparent number of electron transferred (n)	Electron transfer constant (k_0, cm s^{-1})
NDI	-0.09, -0.46	4.77×10^{-6}	1.8	5.73×10^{-3}, 2.07×10^{-2}
NDI-DMe	-0.41	3.63×10^{-6}	1.6	1.51×10^{-3}
NDI-DEtOH	-0.37	4.46×10^{-6}	1.5	4.44×10^{-3}

.

6. Diffusion ordered spectroscopy (DOSY)

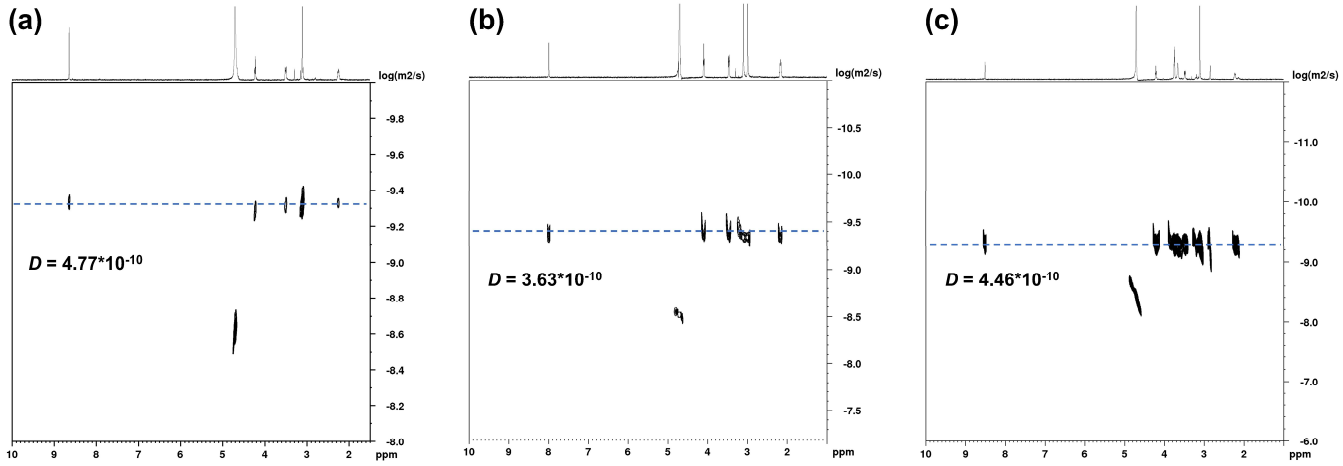

Figure S22. Diffusion-ordered spectroscopy (DOSY) of 1mM (a) **NDI**, (b) **NDI-DMe**, and (c) **NDI-DEtOH** in D_2O with 0.5 M NaCl and corresponding diffusion coefficient *D*.

7. Theoretical calculations

Table S2. HOMO-LUMO, α-HOMO (SOMO) and β-LUMO of napthalene diimide derivatives (Unit: eV)

	HOMO	LUMO	α-HOMO (SOMO)	β-LUMO
NDI^{2+}	-7.3	-3.75	-	-
$NDI^{\cdot+}$			-4.31	-3.05
NDI^{0}	-3.62	-1.03	-	-
$NDI\text{-}DMe^{2+}$	-5.65	-3.23		
$NDI\text{-}DMe^{\cdot+}$			-3.99	-2.8
$NDI\text{-}DMe^{0}$	-3.43	-0.97		
$NDI\text{-}DEtOH^{2+}$	-5.89	-3.44		
$NDI\text{-}DEtOH^{\cdot+}$			-4.12	-2.9
$NDI\text{-}DEtOH^{0}$	-3.52	-1.05		

Atomic labels of **NDI**-derivates

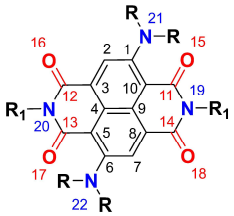

NDI derivates
(R = )

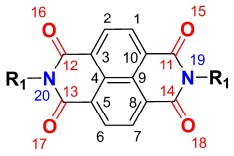

NDI (R = H)

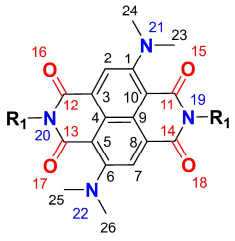

NDI-DMe ($R = N(Me)_2$)

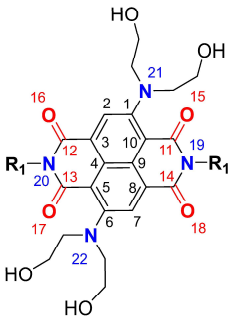

NDI-DEtOH ($R = N(EtOH)_2$)

Table S3. Changes in ADCH charge at relevant atoms of **NDI** upon reduction from $\mathbf{NDI^{2+}}$ to $\mathbf{NDI^{\cdot+}}$ (Omit hydrogen atom)

Atom	ADCH charge		ΔADCH charge
	NDI^{2+}	$NDI^{\cdot+}$	
1(C)	-0.07273	-0.11274	-0.04001
2(C)	-0.07269	-0.1127	-0.04001
3(C)	-0.01615	-0.09372	-0.07757
4(C)	0.002672	0.029144	0.02647
5(C)	-0.01903	-0.09485	-0.07582
6(C)	-0.07147	-0.11207	-0.0406
7(C)	-0.07146	-0.113	-0.04154
8(C)	-0.01918	-0.09572	-0.07654
9(C)	0.002702	0.029991	0.02729
10(C)	-0.01632	-0.09897	-0.08265
11(C)	0.263136	0.244647	-0.01849
12(C)	0.262982	0.237675	-0.02531
13(C)	0.26649	0.235842	-0.03065
14(C)	0.266555	0.247419	-0.01914
15(O)	-0.35343	-0.41128	-0.05785
16(O)	-0.35342	-0.41189	-0.05847
17(O)	-0.35561	-0.41105	-0.05544
18(O)	-0.35562	-0.41439	-0.05877
19(N)	-0.00121	-0.00681	-0.0056
20(N)	-0.00122	0.00056	0.00178

Table S4. Changes in ADCH charge at relevant atoms of **NDI-DMe** upon reduction from **NDI-DMe^{2+}** to **NDI-DMe$^{\cdot+}$** (Omit hydrogen atom)

Atom	ADCH charge		ΔADCH charge
	NDI-DMe^{2+}	NDI-DMe$^{\cdot+}$	
1(C)	0.08938	0.07068	-0.01870
2(C)	-0.13849	-0.08367	0.05482
3(C)	-0.00180	-0.13477	-0.13297
4(C)	-0.03618	-0.07159	-0.03541
5(C)	-0.02841	-0.04355	-0.01514
6(C)	0.08939	0.07028	-0.01911
7(C)	-0.13855	-0.08004	0.05851
8(C)	-0.00178	-0.09983	-0.09805
9(C)	-0.03620	-0.07457	-0.03837
10(C)	-0.02837	-0.04179	-0.01342
11(C)	0.26839	0.32445	0.05607
12(C)	0.19141	0.29131	0.09990
13(C)	0.26843	0.32770	0.05927
14(C)	0.19147	0.25368	0.06221
15(O)	-0.40815	-0.50092	-0.09277
16(O)	-0.37905	-0.42491	-0.04586
17(O)	-0.40816	-0.49998	-0.09182
18(O)	-0.37909	-0.45647	-0.07738
19(N)	0.02678	0.02106	-0.00573
20(N)	0.02680	0.02230	-0.00381
21(N)	-0.06955	-0.19712	-0.12757
22(N)	-0.06952	-0.19799	-0.12847
23(C)	-0.18376	-0.15638	0.02738
24(C)	-0.20128	-0.17261	0.02867
25(C)	-0.18378	-0.15635	0.02743
26(C)	-0.20128	-0.17225	0.02903

Table S5 Changes in ADCH charge at relevant atoms of **NDI-DEtOH** upon reduction from **NDI-DEtOH^{2+}** to **NDI-DEtOH$^{\cdot+}$** (Omit hydrogen atom)

Atom	ADCH charge		ΔADCH charge
	NDI-DEtOH^{2+}	NDI-DEtOH$^{\cdot+}$	
1(C)	0.06434	0.02843	-0.03591
2(C)	-0.04471	-0.02503	0.01968
3(C)	-0.00541	-0.11672	-0.11131
4(C)	-0.03736	-0.00684	0.03052
5(C)	0.02660	-0.08988	-0.11648
6(C)	0.07746	0.05924	-0.01822
7(C)	-0.12211	-0.16010	-0.03799
8(C)	-0.00429	-0.06717	-0.06288
9(C)	-0.03579	-0.09592	-0.06013
10(C)	-0.00952	0.06098	0.07050
11(C)	0.28811	0.32160	0.03349
12(C)	0.19353	0.12971	-0.06382
13(C)	0.21870	0.21869	-0.00002
14(C)	0.20085	0.25264	0.05180
15(O)	-0.40171	-0.44326	-0.04155
16(O)	-0.36048	-0.37513	-0.01465
17(O)	-0.40454	-0.33137	0.07317
18(O)	-0.37155	-0.45671	-0.08516
19(N)	0.02162	0.01142	-0.01020
20(N)	0.01317	0.06653	0.05336
21(N)	-0.07579	-0.09588	-0.02009
22(N)	-0.01175	-0.1948	-0.18305

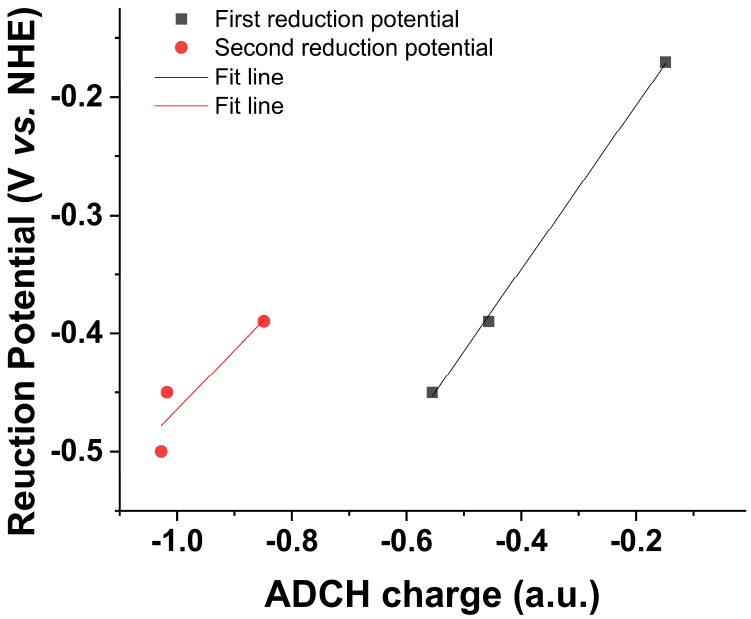

Figure S23. Positive correlation between fragment ADCH charge and molecular reduction potential

Table S6 Population of each type of angular moment atomic orbitals in the single

	s	p	d
NDI$^{\cdot+}$	0.05100	0.92167	0.02733
NDI-DMe$^{\cdot+}$	0.03152	0.94159	0.02689
NDI-DEtOH$^{\cdot+}$	0.01593	0.95594	0.02813

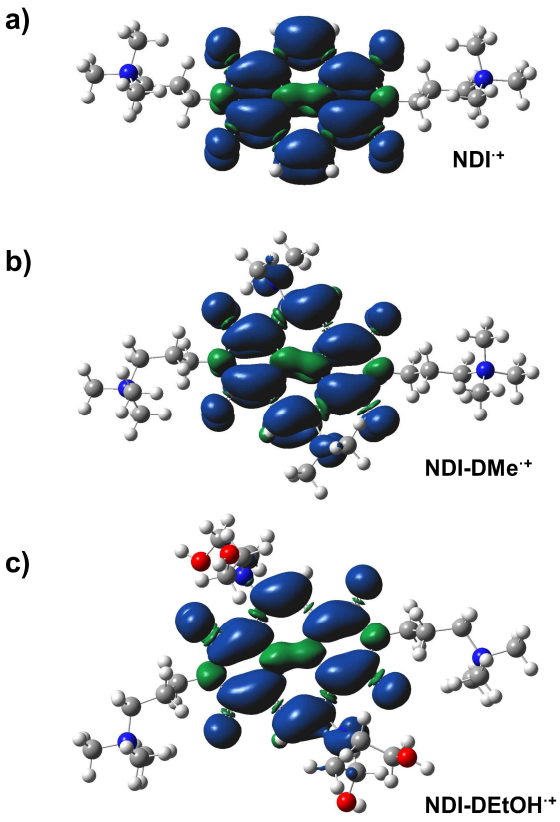

Figure S24. Calculated spin density plots for the radical species of **NDI$^{\cdot+}$, NDI-DMe$^{\cdot+}$, NDI-DEtOH$^{\cdot+}$**

8. Electrostatic potential surfaces

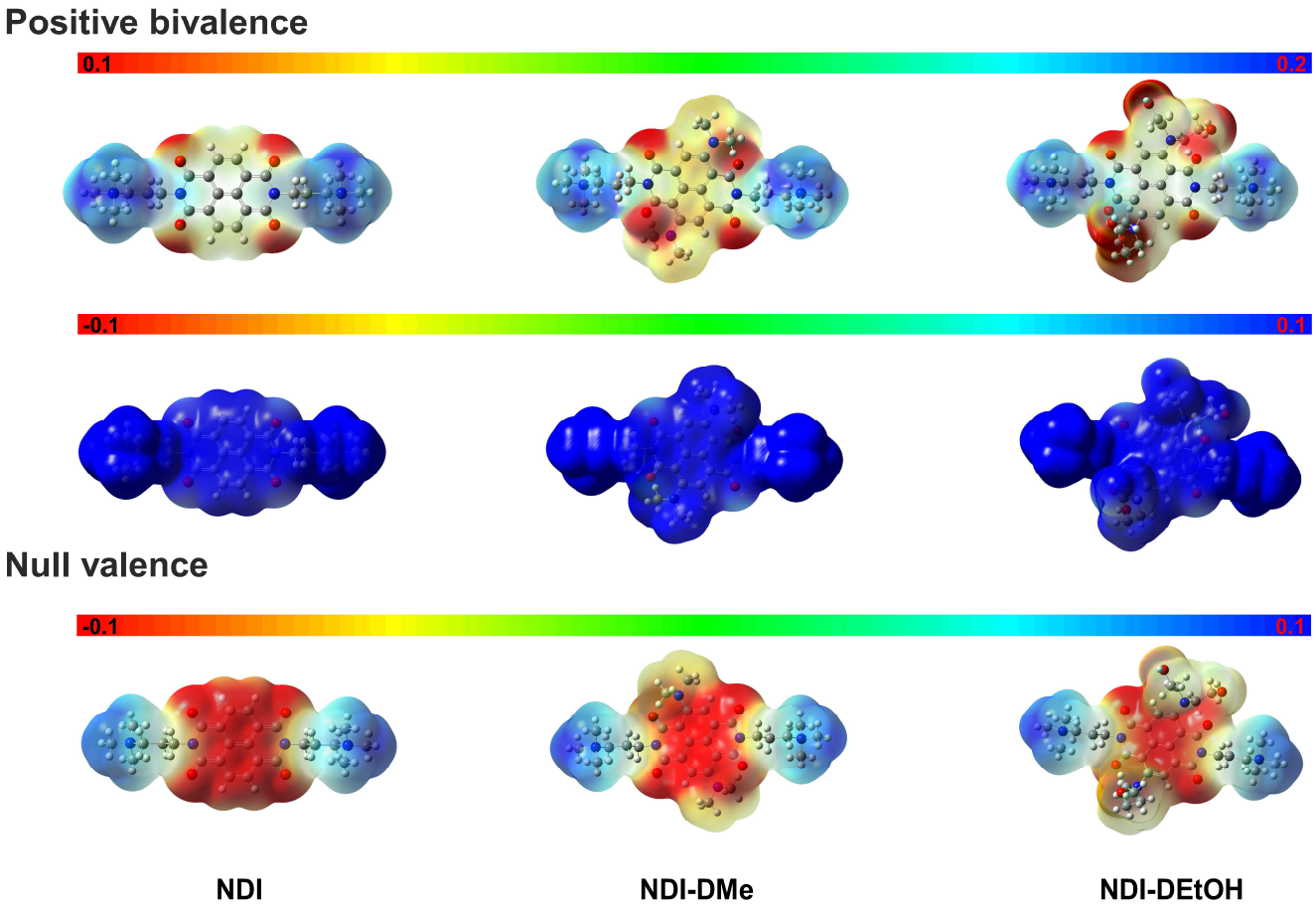

Figure S25. Electrostatic potential surfaces of positive bivlence and null valence of **NDI**, **NDI-DMe**, **NDI-DEtOH**.

9. *In situ* UV-vis experiments

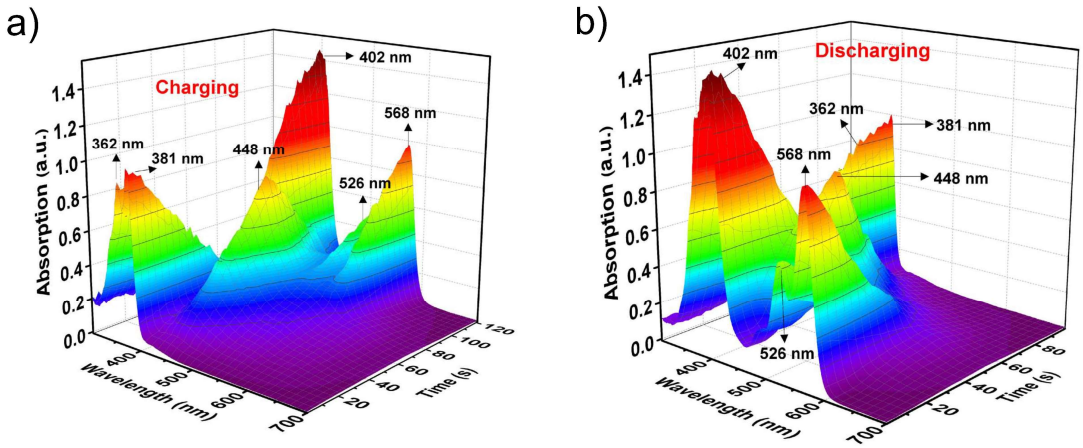

Figure S26. *In situ* UV-vis spectra of (a) charging and (b) discharging processes of **NDI**.[5]

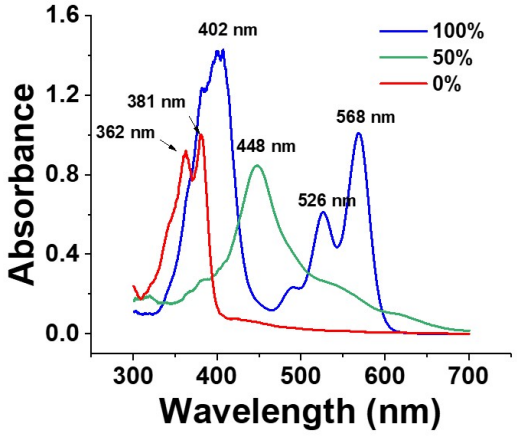

Figure S27. UV-vis spectra of at 0/50/100% SOC of **NDI.**

10. Battery tests

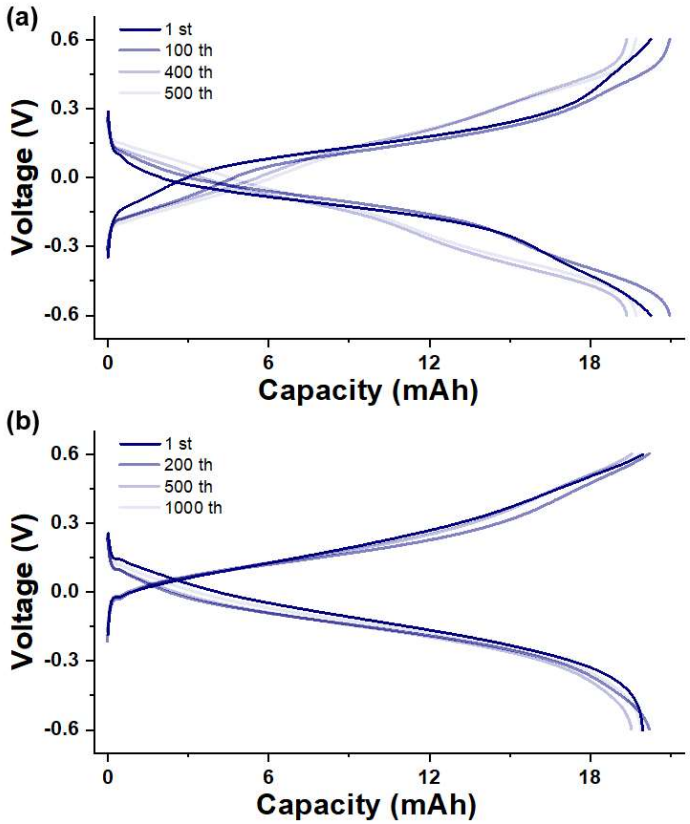

Figure S28. The charge/discharge profiles of (a) **NDI-DMe** and (b) **NDI-DEtOH** in 0.1 M symmetric battery test.

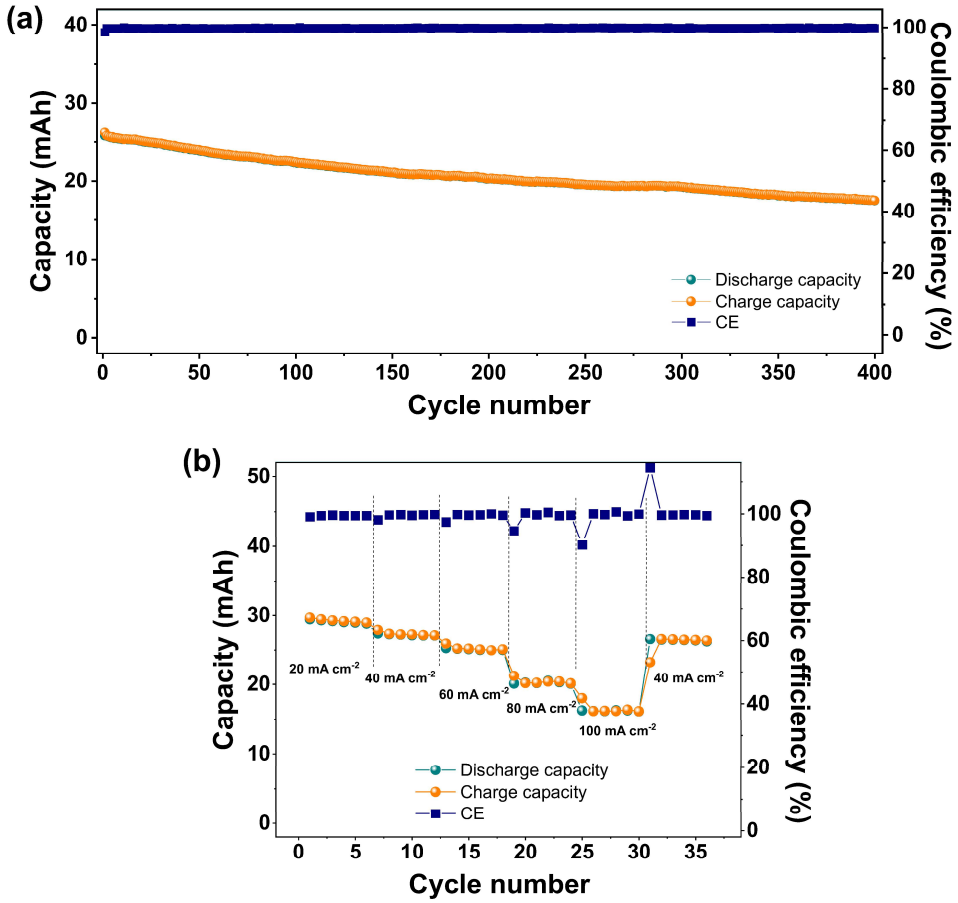

Figure S29. (a) The cyclic performance test at 40 mA cm^{-2} and (b) rate performance test at different current densities (20-100 mA cm^{-2}) of 0.1 M **NDI/FcNCl**-based AORFB.

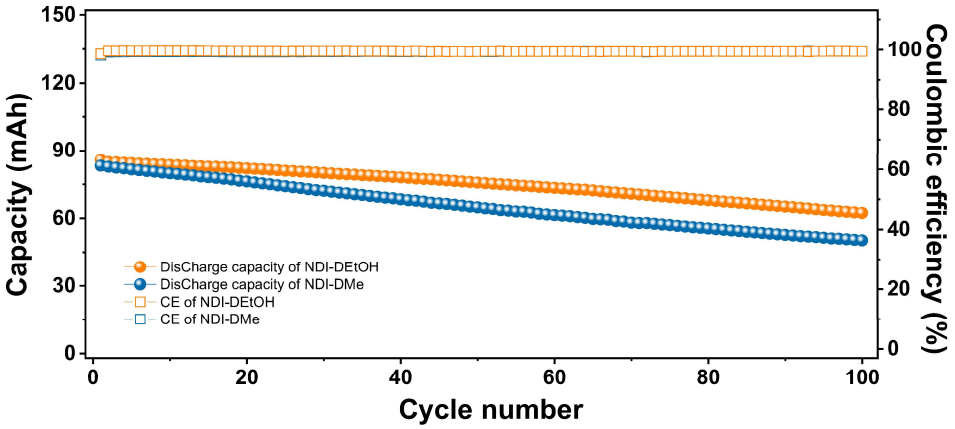

Figure S30. The cyclic performance test at 40 mA cm^{-2} of 0.5 M **NDI-DMe/FcNCl** and **NDI-DEtOH/FcNCl**-based AORFBs.

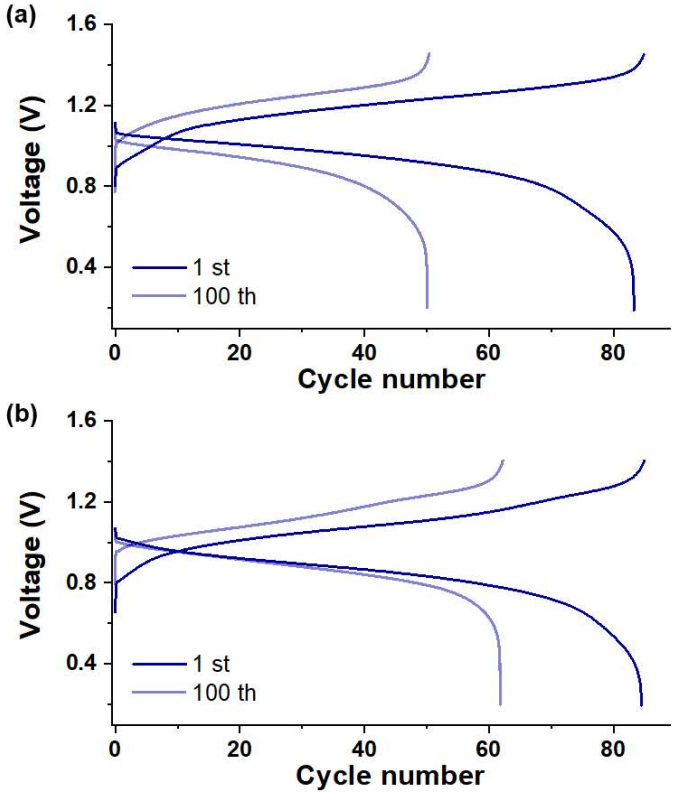

Figure S31. The charging/discharging profiles of 0.5 M (a) **NDI-DMe/FcNCl** and (b) **NDI-DEtOH/FcNCl**-based AORFBs.

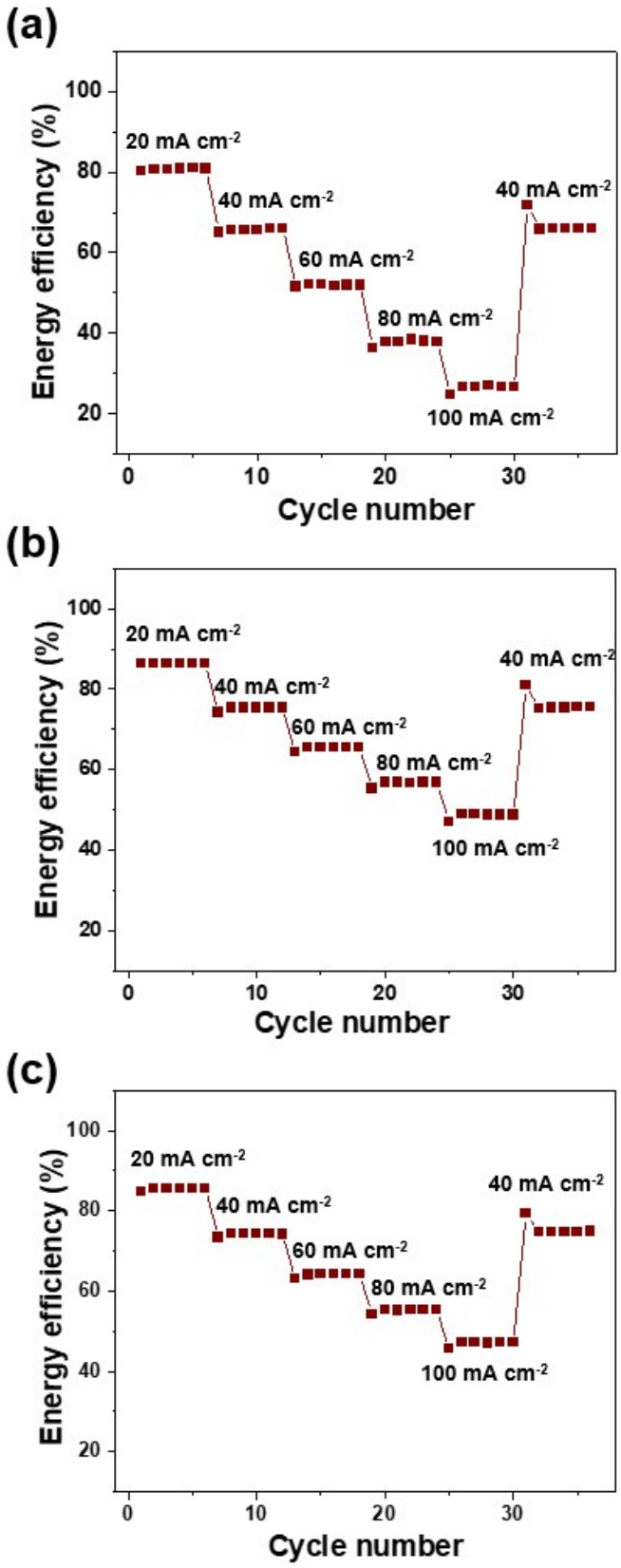

Figure S32. The energy efficiency of 0.1 M (a) **NDI/FcNCl**, (b) **NDI-DMe/FcNCl** and (c) **NDI-DEtOH/FcNCl**-based AORFBs at different current density.

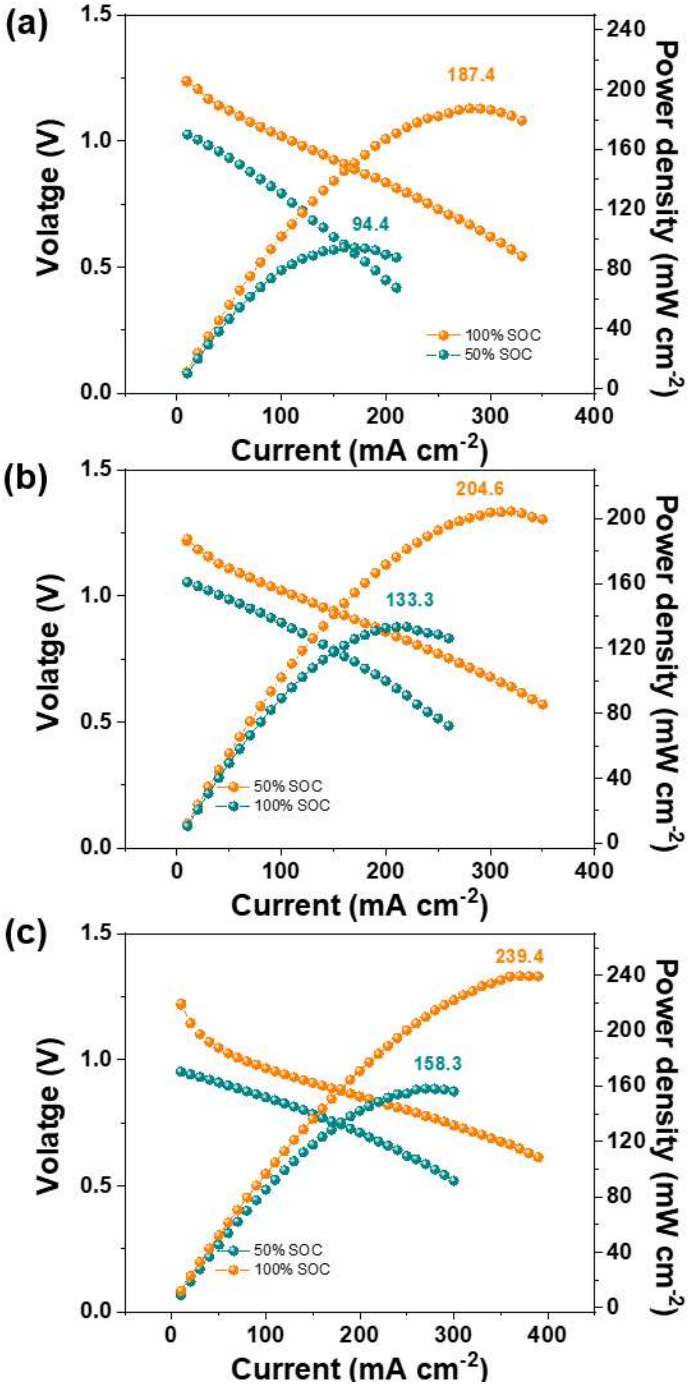

Figure S33. The IR-corrected polarization curves of 0.1 M (a) **NDI/FcNCl**, (b) **NDI-DMe/FcNCl**, (c) **NDI-DEtOH/FcNCl**-based AORFBs without the effect of the membrane resistance (membrane's nominal area-specific resistance is 1.1 Ω cm^2)

11. *In situ* pH test

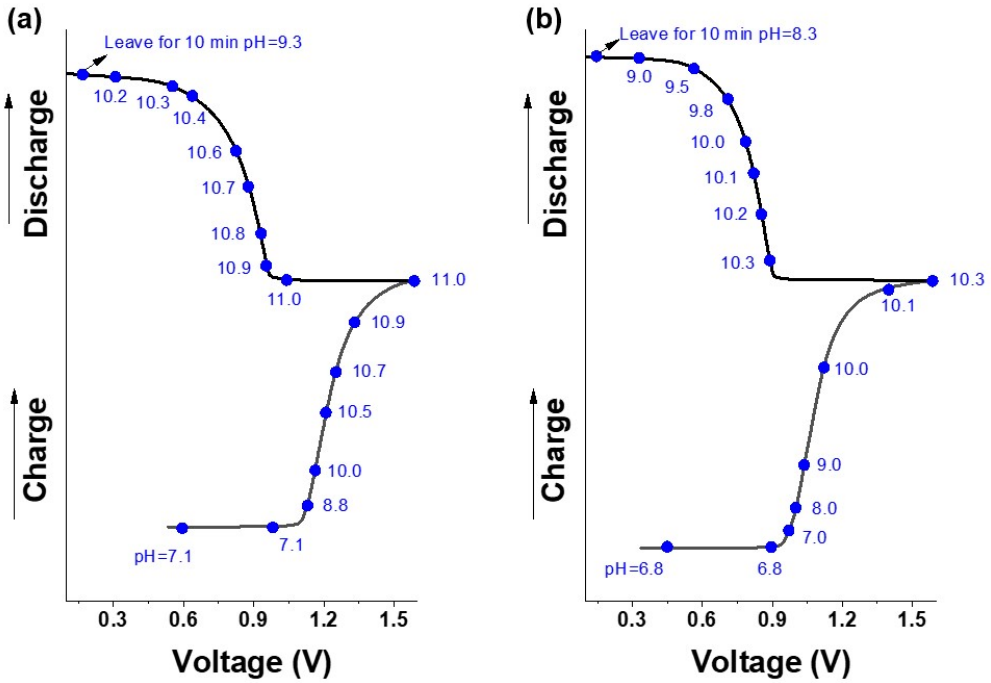

Figure S34. In situ pH test of 0.1M (a) **NDI-DMe/FcNCl** and (b) **NDI-DEtOH/FcNCl** battery anode electrolyte

12. Post-cycling CV

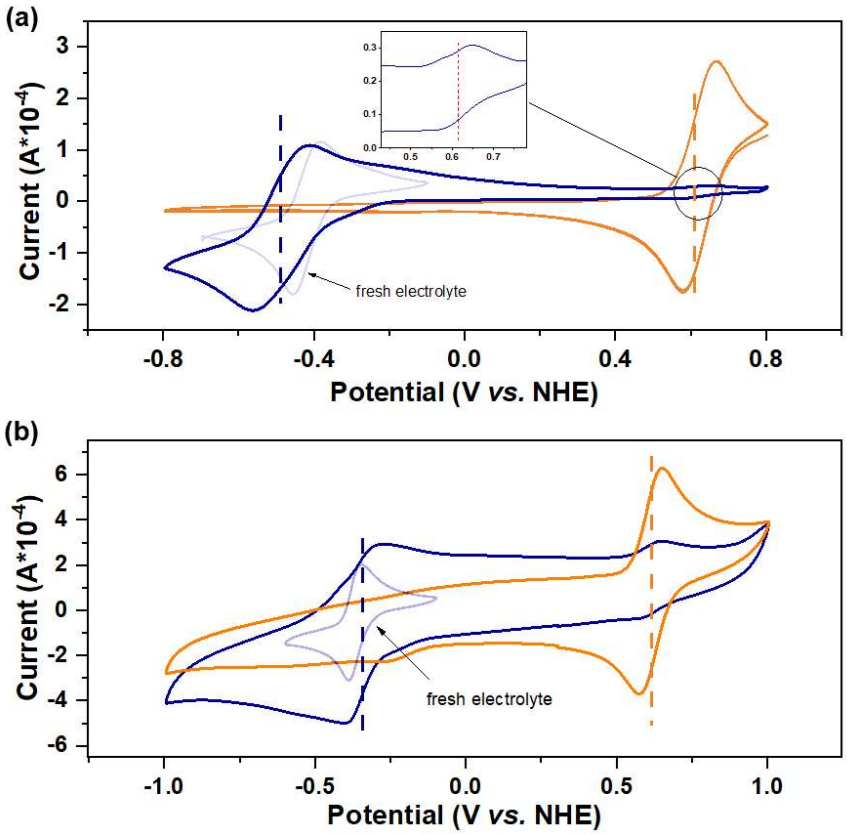

Figure S35. CV curves of 0.1 M (a) **NDI-DMe/FcNCl** and (b) **NDI-DEtOH/FcNCl**-based batteries after cycling.

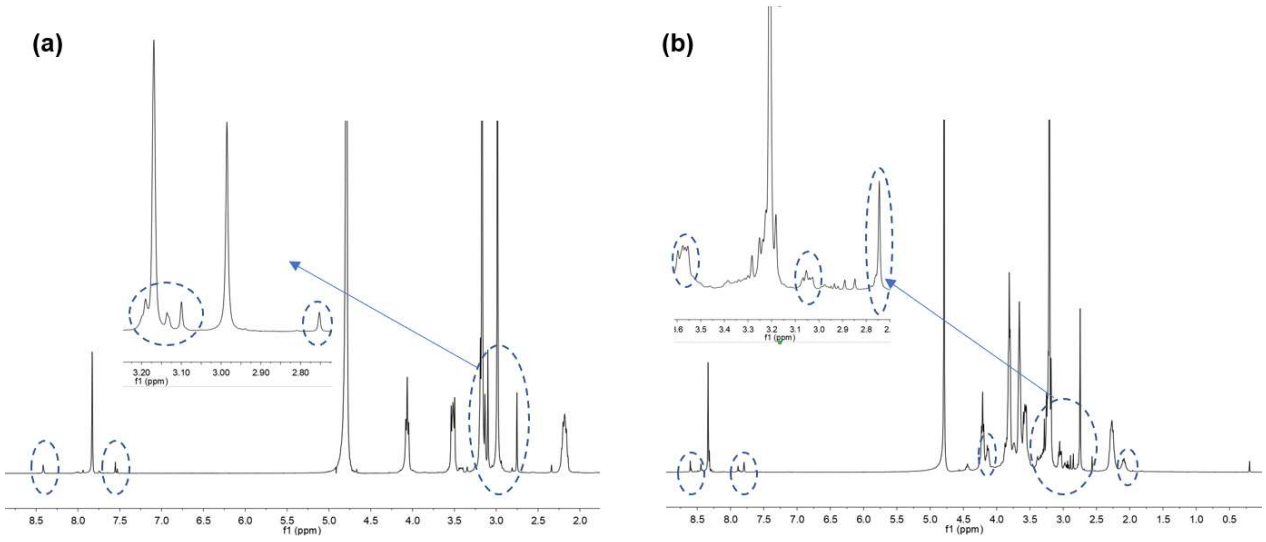

Figure S36. ^{1}H NMR spectra of (a) **NDI-DMe** and (b) **NDI-DEtOH** after 0.1 M AORFBs cycling

13. Summary of various organic anolytes for AORFBs.

Table S7. Summary of various organic anolytes for AORFBs.

Anolyte	Catholyte	Con. active species (Con. electron) (M)	Supporting electrolytes	Membrane	Number of cycles	Cell votage (V)	Current density (mA cm^{-2})	Capacity fade (% per cycle)	Power density (100%/50% SOC) (mW cm^{-2})	Energy efficiency (%)	Ref., Feature
NDI-DMe	FcNCl	0.1 (0.2)	2 M NaCl	DSVN	400	1.02	40	0.07	123.1/94	75.5	This work
NDI-DEtOH	FcNCl	0.1 (0.2)	2 M NaCl	DSVN	400	0.98	40	0.045	128.1/98	74.3	
NDI	FcNCl	0.1 (0.2)	2 M NaCl	DSVN	400	1.07	40	0.08	131.5/	65.6	
NDI	FcNCl	0.1 (0.2)	2 M NaCl	AMVN	350	1.07	40	0.03	98/~70	~60	5
PDI	FcNCl	0.02 (0.04)	2 M NaCl	AMVN	1500	1.06	20	0.0012	--	--	
TPDI	FcNCl	0.05 (0.1)	2 M NaCl	AMVN	2300	0.96	20	0.008	~83/~54	~54	
$4A^{4+}$-NDI	$3I^-/I_3^-$	1.0 (2.0)	1.5 M KCl	Nafion	500	1.15	25	0.004	22.24/--	~48	7
K_2-BNDI	4-OH-TEMPO	0.025 (0.05)	1 M NaCl	AEM	100	1.27	10	--	~37	~57 (at 20 mA cm^{-2})	8
Na_2-BNDI	4-OH-TEMPO	0.04 (0.08)	1 M NaCl	AEM	200	1.27	10	--	--	--	
2H-NDI	BTMAP-Fc	0.05 (0.1)	1 M NH_4Cl 0.5 M NH_4Phos	DSV	320	0.67	10-30	--	--	~42 (at 40 mA cm^{-2})	9
2DMA-NDI	BTMAP-Fc	0.05 (0.1)	1 M NH_4Cl 0.5 M NH_4Phos	DSV	320	0.65	10-30	--	--	~70 (at 40 mA cm^{-2})	
$[(Me)(NPr)V]Cl_3$	FcNCl	0.25 (0.5)	2 M NaCl	AME	50	1.38	60	0.0036	130/63	70	10
$[(NPr)_2V]Cl_4$	FcNCl	0.25 (0.5)	2 M NaCl	AME	100	1.32	60	0.001	92/~40	70	
$[(NPr)_2TTz]Cl_4$	N^{Me}-TEMPO	0.1 (0.2)	2 M NaCl	AMV	300	1.44	40	0.03	--	70	11
$[(NPr)_2FV]Cl_4$	FcNCl	0.1 (0.2)	2 M NaCl	AMV	300	1.42	40	0.06	102/--	~65	12
$[(NPr)_2TV]Cl_4$	FcNCl	0.1 (0.2)	2 M NaCl	AMV	300	1.29	40	0.04	~110/--	64	13
$[(OHPr)_2TV]Cl_2$	FcNCl	0.1 (0.2)	2 M NaCl	AMV	1000	1.18	40	0.0086	120/--	62	
PSPR	$ZnCl_2$	0.1 (0.2)	1 M KCl	Nafion	1018	1.8	20	~0	53/~40	~60 (at 40 mA cm^{-2})	14

"--" indicates that the data is not mentioned in the original literature

The current density conditions for unlabeled energy efficiency are those mentioned in the previous grid

References

1. M. J. Frisch, G. W. Trucks, H. B. Schlegel, G. E. Scuseria, M. A. Robb, J. R. Cheeseman, G. Scalmani, V. Barone, B. Mennucci, G. A. Petersson, H. Nakatsuji, M. Caricato, X. Li, H. P. Hratchian, A. F. Izmaylov, J. Bloino, G. Zheng, J. L. Sonnenberg, M. Hada, M. Ehara, K. Toyota, R. Fukuda, J. Hasegawa, M. Ishida, T. Nakajima, Y. Honda, O. Kitao, H. Nakai, T. Vreven, J. A. Montgomery Jr., J. E. Peralta, F. Ogliaro, M. Bearpark, J. J. Heyd, E. Brothers, K. N. Kudin, V. N. Staroverov, T. Keith, R. Kobayashi, J. Normand, K. Raghavachari, A. Rendell, J. C. Burant, S. S. Iyengar, J. Tomasi, M. Cossi, N. Rega, J. M. Millam, M. Klene, J. E. Knox, J. B. Cross, V. Bakken, C. Adamo, J. Jaramillo, R. Gomperts, R. E. Stratmann, O. Yazyev, A. J. Austin, R. Cammi, C. Pomelli, J. W. Ochterski, R. L. Martin, K. Morokuma, V. G. Zakrzewski, G. A. Voth, P. Salvador, J. J. Dannenberg, S. Dapprich, A. D. Daniels, O. Farkas, J. B. Foresman, J. V. Ortiz, J. Cioslowski, D. J. Fox, *Gaussian 09 Rev. D.01, Gaussian, Inc.: Wallingford, CT,* **2013**.
2. T. Lu and F. Chen, Multiwfn: a multifunctional wavefunction analyzer, *J. Comput. Chem.*, 2012, **33**, 580-592.
3. M. Sasikumar, Y. V. Suseela, T. Govindaraju, Dibromohydantoin: A Convenient Brominating Reagent for 1,4,5,8-Naphthalenetetracarboxylic Dianhydride, *Asian J. Org. Chem.,* 2013, **2**, 779-785.
4. C. G. Tang, M. C. Ang, K. K. Choo, V. Keerthi, J. K. Tan, M. N. Syafiqah, T. Kugler, J. H. Burroughes, R. Q. Png, L. L. Chua, P. K. Ho, Doped Polymer Semiconductors with Ultrahigh and Ultralow Work Functions for Ohmic Contacts, *Nature,* 2016, **539**, 536-540.
5. X. Liu, X. Zhang, C. Bao, Z. Wang, H. Zhang, G. Li, N. Yan, M.-J. Li and G. He, Arylene Diimide Derivatives as Anolyte Materials with Two-Electron Storage for Ultrastable Neutral Aqueous Organic Redox Flow Batteries, *CCS Chem.*, 2023, **5**, 2334-2347.
6. H. Li, H. Fan, R. V. Mahalingam, B. Hu, Y. Feng, J. Song, A Stable Organic Dye Catholyte for Long-life Aqueous Flow Batteries, *Chem. Commun.,* 2020, **56**, 13824-13827.
7. V. Singh, S. Kwon, Y. Choi, S. Ahn, G. Kang, Y. Yi, M. H. Lim, J. Seo, M. H. Baik and H. R. Byon, Controlling π-π Interactions of Highly Soluble Naphthalene Diimide Derivatives for Neutral pH Aqueous Redox Flow Batteries, *Adv. Mater.*, 2023, **35**, e2210859.
8. V. Medabalmi, M. Sundararajan, V. Singh, M. H. Baik and H. R. Byon, Naphthalene Diimide as A Two-Electron Anolyte for Aqueous and Neutral pH Redox Flow Batteries, *J. Mater. Chem. A*, 2020, **8**, 11218-11223.
9. C. Wiberg, L. Evenas, M. Busch and E. Ahlberg, Naphthalene Diimides (NDI) in Highly Stable pH-Neutral Aqueous Organic Redox Flow Batteries, *J. Electroanal. Chem*., 2021, **896**, 115224.
10. C. DeBruler, B. Hu, J. Moss, X. Liu, J. Luo, Y. Sun and T. L. Liu, Designer Two-Electron Storage Viologen Anolyte Materials for Neutral Aqueous Organic Redox Flow Batteries, *Chem*, 2017, **3**, 961-978.
11. J. Luo, B. Hu, C. Debruler and T. L. Liu, A π-Conjugation Extended Viologen as a Two-Electron Storage Anolyte for Total Organic Aqueous Redox Flow Batteries, *Angew. Chem., Int. Ed.,* 2018, **130**, 237-241.
12. M. B. Huang, S. Z. Hu, X. Z. Yuan, J. H. Huang, W. J. Li, Z. P. Xiang, Z. Y. Fu and Z. X. Liang, Five-Membered-Heterocycle Bridged Viologen with High Voltage and Superior Stability for Flow Battery, *Adv. Funct. Mater.,* 2022, **32**, 2111744.
13. X. Zhang, X. Liu, H. Zhang, Z. Wang, Y. Zhang, G. Li, M. J. Li and G. He, Robust Chalcogenophene Viologens as Anolytes for Long-Life Aqueous Organic Redox Flow Batteries with High Battery Voltage, *ACS Appl. Mater. Interfaces,* 2022, **14**, 48727-48733.
14. L. Li, Y. Su, Y. Ji and P. Wang, A Long-Lived Water-Soluble Phenazine Radical Cation, *J. Am. Chem. Soc.,* 2023, **145**, 5778-5785.

Auther Contributions

Gang He and Zengrong Wang conceived the idea for the study. Zengrong Wang and Yawen Li prepared the samples and conducted characterizations. Xu Liu, Xuri Zhang and Heng Zhang conducted electrochemical measurements. Zengrong Wang, Xu Liu, Haiyan Yu and Yujie Zhao completed the full battery tests. Zengrong Wang and Xuri Zhang contributed to the DFT calculations. Zengrong Wang wrote the manuscript. Zengrong Wang, Yawen Li and Gang He revised and polished the manuscript.